



Multi-century tree-ring anatomical evidence reveals increasing frequency and magnitude of spring discharge and floods in eastern boreal Canada

A.F. Nolin^{a,b,c,*}, J.C. Tardif^{b,c}, F. Conciatori^b, S. Kames^b, D.M. Meko^d, Y. Bergeron^{a,c}

^a Institut de Recherche sur les Forêts, Université du Québec en Abitibi-Témiscamingue (UQAT), Rouyn-Noranda, Québec J9X 5E4, Canada

^b Centre for Forest Interdisciplinary Research (C-FIR), The University of Winnipeg, Department of Biology/Environmental Studies & Sciences, 515 Avenue Portage, Winnipeg, Manitoba R3B 2E9, Canada

^c Centre d'Étude de la Forêt, Université du Québec à Montréal (UQAM), CP 8888, Succ. A Montréal, Montréal, Québec H3C 3P8, Canada

^d Laboratory of Tree-Ring Research, University of Arizona, Tucson, AZ 85721, USA



ARTICLE INFO

Keywords:

Climate change
Atmospheric circulation
Dendrohydrology
Earlywood vessels
Fraxinus nigra
Lake Duparquet

ABSTRACT

In eastern boreal Canada, variability in river discharge is poorly understood at the multi-century scale due to short instrumental records. In recent decades, increased magnitude and frequency of spring floods have raised concerns about the potential effects of climate change on flood risk. Unlike tree-ring width, flood rings have a demonstrated dendrochronological utility for reconstructing high discharge in boreal environments. In this study, twelve chronologies of earlywood vessel cross-sectional area (a new hydrological proxy) and ring width were developed from riparian *Fraxinus nigra* trees periodically flooded in spring. These chronologies were used as predictors of Harricana River spring discharge, which was reconstructed for the period 1771–2016. The reconstruction captured 69% of the variance over a 102-year calibration period. The reconstruction indicates that the magnitude and frequency of spring high discharge has increased since the end of the Little Ice Age (1850–1870 CE) and since 1950. The change from a multi-decadal frequency in the late 19th century to a decadal and then interannual frequency in the late 20th century is associated with an increase in snow cover over much of central-eastern Canada. The association between the reconstructed spring discharge and spring atmospheric circulation indices NINO3.4, AMO, NAO may also have changed in these periods and further work is needed to assess the stability of these associations. The correlation between reconstructed and instrumental spring discharge at the regional scale, as well as the shared features in reconstructed discharge and other paleorecords from subarctic Québec suggest a common hydrological signal across the study area and for the early 20th to 21st centuries. The unprecedentedly low and high spring discharge in recent decades compared to the historical natural variability of the last 250 years also suggests that the increase in flood frequency and magnitude originates from climate change.

1. Introduction

Climate extremes and exceptional floods are becoming more frequent worldwide (Berghuijs et al., 2017; Kundzewicz et al., 2019) and particularly in Canada (Burn et al., 2016; Buttle et al., 2016; Burn and Whitfield, 2015, 2018; Bush and Lemmen, 2019). Over the last decade (2010–2020), flooding has emerged as the costliest natural disaster in Canada with insurance payouts exceeding one billion Canadian dollars per year (IBC, 2020). The 2019 floods in Ontario (McNeil, 2019) and Québec (ECCC, 2020) surpassed the 2017 flood level considered, at the time, as the 100-year flood in the Ottawa River basin (Turcotte et al.,

2019; ECCC, 2020). Given that most Canadian communities are located close to water bodies, and given the reliance on hydropower in the country, there is an urgent need to plan for future resilience of water and flood security management to climate change (Winsemius et al., 2016; Cherry et al., 2017).

In Canada, observed global warming and projections from greenhouse gases emission scenarios indicate a rate of warming about twice as fast as that projected for the rest of the Northern Hemisphere (Vincent et al., 2018; Bush and Lemmen, 2019). The majority of floods in Canada are generated by either intense rainfall, snowmelt or ice melt (Buttle et al., 2016; Burn et al., 2016; Burn and Whitfield, 2018). In northern

* Corresponding author at: Institut de Recherche sur les Forêts, Université du Québec en Abitibi-Témiscamingue (UQAT), Rouyn-Noranda, Québec J9X 5E4, Canada.

E-mail address: alexandreflorent.nolin@uqat.ca (A.F. Nolin).

Canadian watersheds where discharge is determined by the accumulation and melting of snow and ice, flooding results from a complex combination of excess rain and snow, rain-on-snow events or ice jams and the magnitude of temperature jump from winter to spring (Javelle et al., 2003; Aygün et al., 2019). However, so far, no consistent trend in mean or extreme annual precipitation or in annual discharge has been observed for Canada as a whole (Aygün et al., 2019). In northern Canada, and particularly in winter, an increase in annual precipitation relative to snowfall, was observed (Vincent et al., 2018). Seasonal snow cover is also projected to decrease during the 21st century with a later snow onset and an earlier spring snowmelt (Bush and Lemmen, 2019). This trend is visible in the ice freeze-up and break-up records for south-central Ontario, where a longer ice-free period has been observed since the 1900's related to the seasonal temperature warming (Fu and Yao, 2015). Analysis of Canada-wide instrumental discharge data indicates that the timing and magnitude of seasonal maxima has shifted toward higher winter discharge and earlier spring snowmelt since 1950 (Mortsch et al., 2015). This is consistent with the observed change in the seasonality of river input to the Hudson Bay between 1968 and 2008; with an increase in winter discharge, a decrease in summer discharge, and an increase in maximum annual discharge being observed since the mid-1980s (Déry et al., 2011).

From a climate change perspective, i) a decrease in snow accumulation would lead to a reduction in the magnitude of snowmelt flooding, whereas ii) an increase in extreme precipitation events would lead to an increase in rain associated to flooding. Hydrological simulations using outputs from regional climate models for northern Québec and Ontario (Guay et al., 2015; Wang et al., 2015; Clavet-Gaumont et al., 2017) suggest that by 2050 rain and snow amounts will contribute more to discharge in the winter and fall months and less to discharge in the summer months than during the 20th century. Increases in the magnitude of hydrological extremes are also expected but it remains uncertain how the projected change in climate will affect flood frequency and magnitude (Gaur et al., 2018). Gaur et al. (2019) showed from simulations that under various climate change scenarios about 40 to 60 of the 100 most populous Canadian cities are expected to experience increasingly frequent flooding by 2100, particularly in coastal areas, southern Ontario and northern Canada. For example, in Toronto, the return period of the historic 100-year flood would be reduced to a return period of 22 to 30 years under a minimum climate change scenario (RCP 2.6).

The uncertainties in projecting future hydroclimatic trajectories limit flood risk estimations currently based on instrumental records of natural discharge (Mortsch et al., 2015; Buttle et al., 2016). Unfortunately, because of technical and economical limitations, the hydrological records in northern Canada are of short length and highly dispersed in space (Koshida et al., 2015; Pellerin, 2019). Also, because most Canadian hydropower capacity is located in the North (Cherry et al., 2017), the influence of dams on lakes and rivers complicate the analysis of climate change impacts using these short instrumental records (Ljungqvist et al., 2016). It is thus particularly important to extend the existing discharge data spatially and temporally in these regions. Simulations from the north of Finland have shown that more frequent freeze-thaw episodes and ice-flooding in winter or spring could threaten the integrity of hydroelectric facilities or force them to divert floodwaters more often to spillways instead of generating power (Gebre et al., 2014). To improve planning for the economic and social impacts of future climate change, it is essential to understand whether recent changes in discharge and flooding in eastern boreal Canada are part of the historical natural variability or whether they are unprecedented and associated with recent climate change.

Paleoindicators can provide proxy data to complement short instrumental discharge records and help place them in a historical perspective (Saint-Laurent, 2004; Baker, 2008; Meko and Woodhouse, 2011; Ballesteros-Cánovas et al., 2015; Wilhelm et al., 2019). Among the paleoflood indicators, tree rings can be considered an excellent hydrological proxy due to the interconnection among climate, hydrology and

tree growth, and tree-ring chronologies are annually resolved and continuous series (Meko and Woodhouse, 2011; Meko et al., 2012). In semi-arid environments, where water deficit is a major factor limiting tree growth, ring-width chronologies have been successfully used to reconstruct past discharge and especially low discharge (Meko et al., 2001; Woodhouse et al., 2006; Biondi and Meko, 2019; Martínez-Sifuentes et al., 2020). In contrast, in boreal environments where water is not as limiting to tree growth, the relationship between tree-ring width and discharge may not be as clear (Tardif et al., 1998; Kames et al., 2016). Ring-width chronologies integrate many environmental factors and extracting a specific flood signal can be complex or difficult (Boucher et al., 2011; Agafonov et al., 2016). In addition, if spring thaw occurs before the start of the growing season, ring-width chronologies may not register variations related to high spring water levels. In a northern Québec reservoir, Nicault et al. (2014) showed that spring discharge was difficult to reconstruct using a combination of ring widths, earlywood density and stable isotope chronologies mainly because flooding occurred during the period of tree dormancy. The authors had better results when including ice-scar frequency in their reconstruction. Indeed, spring flooding in Northern Québec has been reconstructed mostly by studying the physical injuries (scars) left on shoreline trees by the abrasion of floating ice and debris during spring break-up (Tardif and Bergeron, 1997b; Bégin, 2001; Lemay and Bégin, 2008; Boucher et al., 2011; Nicault et al., 2014).

The study of the anatomy of growth rings in trees directly exposed to seasonal floods can provide quantitative and continuous predictors of seasonal discharge in boreal regions. Anatomical changes in earlywood vessels associated with the physiological response to anoxia during persistent flooding (hereafter referred as flood rings) have been noted in riparian ring-porous trees (*Fraxinus sp.*, *Quercus sp.*) following major flood years (Astrade and Bégin, 1997; St. George and Nielsen, 2000; Tardif et al., 2010; Kames et al., 2016; Nolin et al., 2021). Recent work (Meko et al., 2020; Dickson, 2020) indicate that in riparian diffuse-porous trees (*Salix sp.*, *Populus sp.*) flooding also lead to the development of tree-ring anomalies (anatomical irregularities). Flood rings have also been experimentally reproduced and been shown to form when ring-porous trees are flooded during the period of earlywood vessels formation (Copini et al., 2016; Tardif unpublished data). Flood rings are characterized by either an increase in earlywood vessel number and/or a reduction in earlywood vessel cross-sectional areas according to species (St. George and Nielsen, 2000; Copini et al., 2016; Kames et al., 2016; Nolin et al., 2021). The timing and duration of flooding relative to the period of earlywood vessel formation and sample location along the tree stem are factors that influence flood-ring formation (St. George et al., 2002; Copini et al., 2016).

Flood rings have been successfully used to detect major floods (St. George and Nielsen, 2003; Wertz et al., 2013; Therrell and Bialecki, 2015; Meko and Therrell, 2020; Nolin et al., 2021) but few studies have used continuous year-to-year measurements of earlywood vessels to study hydroclimate variability (Tardif et al., 2010; Kames et al., 2016). Recently, Meko and Therrell (2020), in addition to visual identification of flood rings, measured the width of the first row of earlywood vessels in ring-porous overcup oak (*Quercus lyrata* Walt.). This work allowed effective reconstruction of spring floods in the White River, Mississippi. López et al. (2014) reconstructed summer and annual discharge of the Atrato River, Columbia, from the number of vessels in the annual tree ring in the diffuse-porous *Priaria copaifera*. The authors found that in the equatorial forest, the number of vessels in the annual ring tends to be higher and the total ring width greater in flood years than in dry years. On the other hand, Kames et al. (2016) demonstrated that in the boreal forest of Lake Duparquet, earlywood vessel chronologies from ring-porous black ash (*Fraxinus nigra* Marsh.) were more effective than ring width in capturing the variability of low and high spring discharge. These results support the utility of developing long earlywood vessel chronologies from floodplain trees as proxy records of river discharge and flooding. Tree-ring anatomical sequences from trees growing

directly on floodplains may also allow reconstruction of the full range of spring discharge variability in boreal environments.

The objectives of this study are twofold. First is the multi-century reconstruction of annually resolved spring discharge from hydrological proxies: ring width and cross-sectional area of earlywood vessels from *F. nigra* trees growing on the floodplain of Lake Duparquet. Second is investigation of the temporal stability of the reconstruction and determination of the main climatic and large-scale atmospheric circulation drivers associated with multi-century spring discharge variability.

2. Materials and methods

2.1. Study area

The study was conducted on Lake Duparquet ($48^{\circ}28' \text{ N}$, $79^{\circ}16' \text{ W}$; Fig. 1) located in the Clay Belt of both Northern Ontario and Québec (Daubois et al., 2015). Lake Duparquet forms a 50 km^2 waterbody draining north into the James Bay through the Abitibi River (Tardif and Bergeron, 1997b). The rivers feeding Lake Duparquet are not regulated by dams, making it a unique site for the study of long-term flood dynamics in a watershed in which hydroelectric dams have been present downstream since the 1910s (CEHQ, 2019; Hydro-Québec, 2019). The closest dam to Lake Duparquet is located 140 km downstream (Iroquois Falls dam, built in 1914) and regulates Lake Abitibi (OMNRF, 2019;

OPG, 2019). A natural steep rapids 5 km downstream of Lake Duparquet (Rapide Danseur) prevents any effect of downstream dams or regulation on the lake level.

Lake Duparquet is situated at the southern fringe of the boreal eco-zone where forests can be characterized by an association of balsam fir (*Abies balsamea* (L.) Mill.), black spruce (*Picea mariana* (Mill.) BSP), paper birch (*Betula papyrifera* Marsh.), white spruce (*Picea glauca* (Moench) Voss) and trembling aspen (*Populus tremuloides* Michx.) (Denneler et al., 1999). *Fraxinus nigra* can be found in waterlogged areas and riparian forests in pure stands (Tardif and Bergeron, 1997a) or in association with eastern white-cedar (*Thuja occidentalis* L.) and occasionally balsam poplar (*Populus balsamifera* L.) (Denneler et al., 1999; Tardif and Bergeron, 1992; Tardif and Bergeron, 1999). The soils of the region are dominated by deposits from the Quaternary Ojibway lake and by glacial till that transitions into peatlands northward (Daubois et al., 2015). The very flat and clayey banks of Lake Duparquet are flooded each spring for a period ranging from a few days to months and are largely colonized by *F. nigra*. The species can reach an age of 250 years in these forests (Tardif and Bergeron, 1999).

Lake Duparquet area has a sub-boreal climate with a mean annual air temperature of 0.7°C , mean annual precipitation of 890 mm and mean annual snowfall of 250 mm for the period 1971–2000, as indicated by data from La Sarre weather station data ($48^{\circ}48' \text{ N}$, $79^{\circ}11' \text{ W}$; Fig. 1) obtained from Canadian Climate Normals (http://climate.weather.gc.ca/climate_normals). Precipitation peaks occur in spring and fall, and

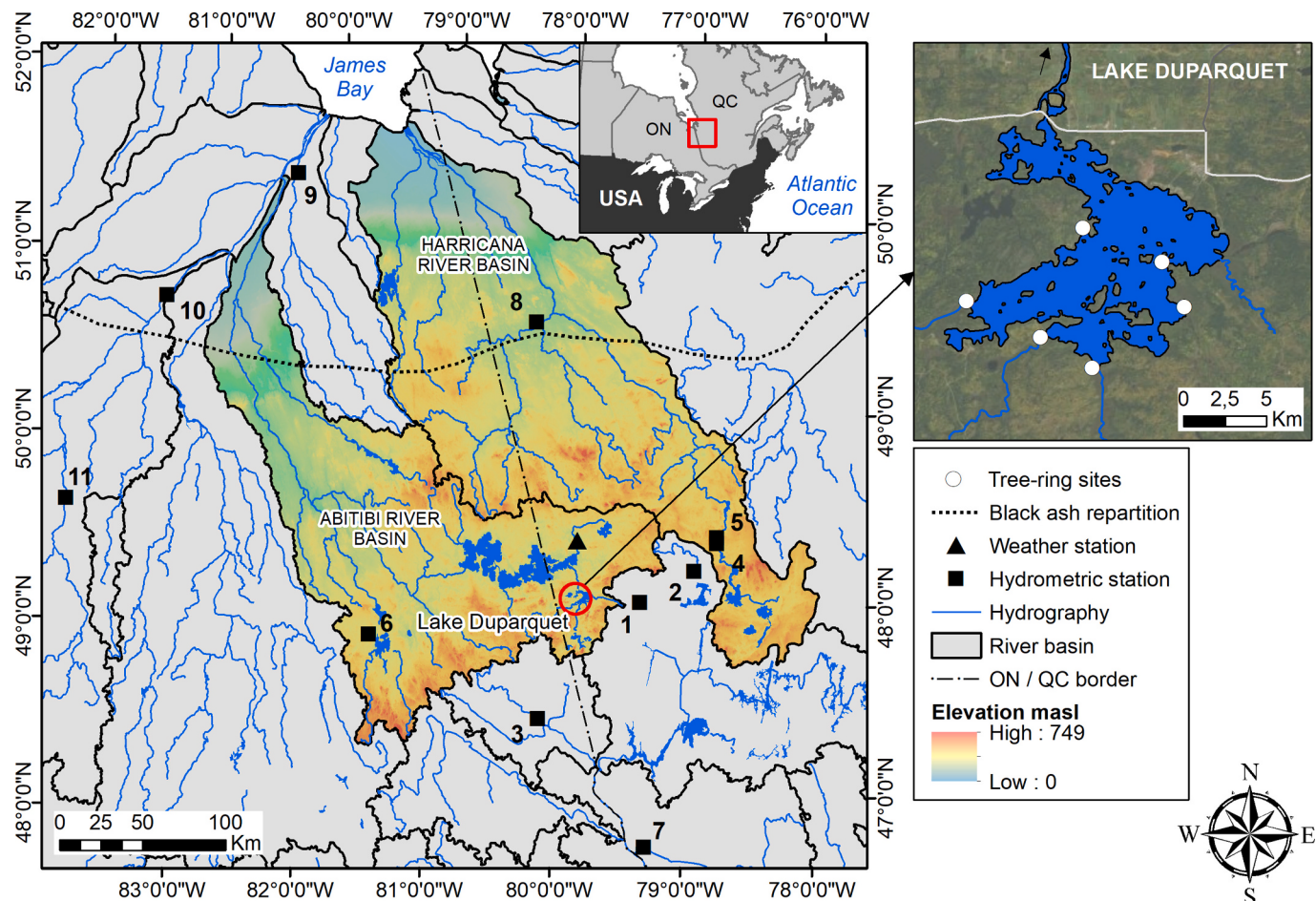


Fig. 1. Map of the study area. Geographic location of the study area at the border between Ontario (ON) and Québec (QC), in Canada (left panel upper inset). Lake Duparquet (red circle in left panel) is located at the head of the Abitibi River basin. Discharge record reconstructed is at Harricana River (black squares No. 4 & 5) on the upper reach of Harricana River. Other hydrological stations are listed by their numbers in Table 1. The upper right inset shows locations of riparian *Fraxinus nigra* sampling sites at Lake Duparquet (white dots). (For interpretation of the references to colour in this figure legend, the reader is referred to the web version of this article.)

persistent winter snowpack is common until the month of May (Supplementary Fig. S1a). Lake Duparquet is not equipped with a hydrologic station, but its hydrology is comparable to that recorded on the Harricana River ($48^{\circ}34' \text{ N}$, $78^{\circ}07' \text{ W}$; Fig. 1) located 85 km to the east (Tardif et al., 2010; Kames et al., 2016). Both show a boreal regime driven by mixed snow and rain processes. At the end of the ice season, the winter snowpack melts and rapidly transforms the low winter discharge into a spring freshet peak. The spring breakup flood usually occurs in May and its average contribution to annual discharge ranges from 11 to 30% for the period 1915–2020 (Water Survey of Canada, <https://wateroffice.ec.gc.ca>; Supplementary Fig. S1b). Spring recession magnitude and summer precipitation generally contribute to high summer discharge. In the fall, small floods may be triggered by episodes of intense rainfall, prior to a return of river ice and accumulation of snow in winter.

2.2. Sample collection, measurement and crossdating

In summer 2017 and 2018, 125 increment core samples from 65 trees were collected from *F. nigra* sites exposed to periodical flooding on Lake Duparquet. Cores were collected from living trees using a 5 mm increment borer and discs were collected from old logs or fallen trees. This sampling aimed to update existing *F. nigra* anatomical and ring-width chronologies from Lake Duparquet (Tardif and Bergeron, 1993; Kames et al., 2016; Tardif et al., 2016). Because flood rings were reported to occur below the water level at the onset of earlywood formation (St. George et al., 2002; Copini et al., 2016) samples were collected as close as possible to the ground. Wood samples were prepared according to standard dendrochronological techniques (Phipps, 1985; Cook and Kairiukstis, 1990) and were sanded on a series of progressively finer grit up to P600 grade. After cleaning with pressurized air, the sample surfaces were rubbed with white chalk to increase the contrast between the vessels and the other cell types (Tardif and Conciatori, 2006; Kames et al., 2016). Tree rings were visually crossdated using the pointer-years developed for *F. nigra* on Lake Duparquet (Tardif and Bergeron, 1993; Kames et al., 2016) and the list method (Phipps, 1985).

Given that *F. nigra* trees seldom reach many centuries in age (Tardif and Bergeron, 1999), the oldest and best well-preserved wood samples from Tardif and Bergeron (1993) (11 cores from 9 trees) and from those collected in 2017 (13 cores from 13 trees) were selected for image analysis and anatomical measures. Given our objective to reconstruct discharge at the multi-century scale, the oldest samples showing clear tree rings with no rot or missing sections were selected after inspection under a stereomicroscope. The pre-existing anatomical series from Kames et al. (2016) (40 cores from 20 trees) and Tardif et al. (2016) (4 cores from 4 trees) were also used. Anatomical measurements were produced from high-resolution pictures using procedures similar to those described in Tardif and Conciatori (2006) and Kames et al. (2016). The prepared surfaces were scanned by a digital camera (Nikon DS-Fi1) mounted on a stereomicroscope (Nikon SMZ1000) to obtain standardized images (TIFF format, $20\times$ magnification, 1600×1200 dpi) of the tree rings. Pictures were then processed with the Canny (1986) edge detection algorithm with ImageJ2X (Rueden et al., 2017) to automatically delineate the vessel shapes. Each output image was then manually corrected using a graphics tablet to verify and improve vessel identification. Incomplete areas of lumen at the edges of cores or images were excluded from the analysis. Once each vessel shape was clearly delineated, the boundary between early and latewood was qualitatively identified as the interruption of the largest vessels (Tardif and Conciatori, 2006; Kames et al., 2016). Each ring was analyzed with WinCell Pro v2018c (Régent instrument, 2018) on vessels with a cross-sectional area greater than $3000 \mu\text{m}^2$ (Tardif, unpublished data). For each tree-ring sample, 12 continuous variables were measured, including 8 anatomical variables and 4 ring-width variables.

Anatomical variables were mean (MVA) and total vessel lumen cross-sectional area (TVA) within the earlywood, number of vessels (N), mean

vessel area of the 25% largest (L25) and smallest vessels (S25), porosity within the earlywood (pE) (defined as $\frac{\text{TVA}}{A}$, with A the earlywood area), density of vessels in the earlywood (dE) (defined as $\frac{N}{A}$), and hydraulic diameter (Dh) (defined as $\left(\frac{\sum D_i^4}{N}\right)^{\frac{1}{4}}$ with D_i equivalent circle diameter (in meter) expressed as $\sum_{i=1}^n D_i = 2\sqrt{\frac{A}{\pi}}$ from the Hagen-Poiseuille law (Tyree and Zimmermann, 2002). Hydraulic diameter is a more physiologically-based expression of water transport in trees than vessel conductance area (Scholz et al., 2013), whereas the S25 and L25 chronologies separate the signals that may be carried by different classes of vessels size (García-González and Fonti, 2006).

Ring-width variables were the total ring width (RW), earlywood width (EW), and latewood width (LW) (defined as $RW-EW$), and the proportion of earlywood within the total ring-width (EW%RW) (defined as $\frac{EW}{RW}$). The EW was measured with WinCell as it was more appropriate for suppressed years, but the RW was measured with CooRecorder (Larsson, 2003b), and LW resulted from their difference.

Because the anatomical measurements of tree-ring series (L25, S25, MVA, TVA, pE, N, dE and Dh) were designed to extend the existing chronologies (Kames et al., 2016; Tardif et al., 2016) back in time and considering that image analyses are time-consuming, the measurements did not include years after 1950 for 9 series. Tree-ring width measurements (EW, LW, RW, EW%RW), however, were conducted over the entire period of time available.

2.3. Chronology development

The quality of crossdating and measurement of each of the ring-width series (43 trees \times 12 variables) was inspected in CDendro (Larsson, 2003a) and COFECHA (Holmes, 1983) prior to analysis. Series detrending and chronology development were computed using the ‘dplR’ package (Bunn, 2008) in R environment (R Core Team, 2020). Some 302 missing values (representing 0.43% of the total measurements) related to rotten parts in the oldest samples were interpolated using the spline filling function in ‘dplR’ package. Once the series were completed and quality-checked, a detrending was performed to remove low-frequency age-related or stand-related dynamics and to retain mainly high-frequency variations (Cook and Kairiukstis, 1990). Individual tree-ring series were divided by a cubic smoothing spline function with a 50% frequency response at 60 years (Kames et al., 2016). The spline function rigidity was set at 30 years for 0.19% (41/516) of the series i.e.; when adverse effects at the start or at the end of the series (extremely high values) were observed. Series with significant autocorrelation were prewhitened using a best-fit autoregressive model (Cook and Kairiukstis, 1990) to produce residual chronologies. When autocorrelation was found to be non-significant, the standard chronology was preferred (Kames et al., 2016). Finally, to lower the influence of outliers, detrended series for individual cores were averaged into site chronologies using a biweight robust mean (Cook and Kairiukstis, 1990). Temporal coherence among series was assessed with the inter-series correlation coefficient (Rbar), and adequacy of sample size was assessed with the subsample signal strength (SSS; Wigley et al., 1984; Cook et al., 1999). The Rbar statistic expresses the mean correlation between all possible pairs of the individual tree-ring series, while the SSS reflects the loss of common variance between the series due to the decrease in sample size back in time (Wigley et al., 1984; Cook et al., 1999).

2.4. Reconstruction of spring discharge

Based on Kames et al. (2016), linear regressions were computed between discharge variables (predictand) and tree-ring chronologies (predictors) in exploratory analyses. For the common period 1915–2016, the best linear correlation between the Lake Duparquet

MVA chronology and the Harricana River discharge was found with the mean discharge from April 15 to June 30 ($r = -0.79, p < 0.001$), which was therefore chosen as the variable to be reconstructed (hereafter, Harricana spring discharge).

Two stepwise multiple linear regression models were developed to reconstruct Harricana spring discharge using the R package 'Olsrr' (Hebbali, 2020). In the first model (REC1) the 12 predictor chronologies were transformed using principal components analysis (PCA) to overcome multicollinearity issues among predictors (Hidalgo et al., 2000; Woodhouse et al., 2006). PCA was performed on a correlation matrix with the R base environment for a 1771 to 2016 common period, and the number of statistically significant principal components (PC) to be used as predictors of discharge was selected by a broken stick model (Legendre and Legendre, 2012). To account for autocorrelation in tree-ring time series, because tree growth is influenced by climate conditions prevailing during the current and the previous growing season, lagged PC (-1, 0, +1 year) were introduced in regression series (Cook and Kairiukstis, 1990; Meko and Graybill, 1995). The second model (REC2) consisted of the 8 anatomical and 4 ring-width chronologies and their lags (-1, 0, +1) without PCA transformation.

2.5. Model performance

Model assumptions were checked with a standard analysis of residuals, and the final models were validated using a split-sample procedure (Snee, 1977; Cook and Kairiukstis, 1990). This cross-validation technique consists of dividing the period of overlap between instrumental discharge data and tree-ring chronologies into two sets of half-calibration and verification of equal length. A first half (1915–1965) was used to calibrate the model, and the second half (1966–2016) was used to verify the model. This procedure was then inverted (1966–2016 for calibration, 1915–1965 for verification). The overall performance of the models was estimated using the adjusted explained variance (adjR^2) from calibration, as well as the reduction of error statistic (RE; Briffa et al., 1988) and the coefficient of efficiency (CE; Cook and Kairiukstis, 1990) from validation. Agreement between the reconstructed estimates and instrumental data was estimated with the conventional statistics of root-mean-square error and mean-absolute error (RMSE, MAE; Cook et al., 1999) and the sign test and product-mean test (PMT) calculated on z-scores (Cook and Kairiukstis, 1990). These statistics provide information on the ability of the models to reconstruct the discharge not used in model fitting. In addition, the daily hydrographs of the Harricana spring discharge (April 15 to June 30, calculated for 1915–2020) were submitted to a K-Means clustering analysis (Legendre and Legendre, 2012) to further assess the model performance in reconstructing extreme low and high discharge associated with individual clusters.

2.6. Climate and large-scale atmospheric circulations relationships to spring flooding

To assess the degree of association between the reconstructed spring discharge and current climatic data, hydrological data, large-scale atmospheric circulation indices and existing hydrological reconstructions from subarctic Québec, simple and bootstrapped Pearson correlations were calculated. The stationary bootstrapped correction avoids bias in variance from multiple spatial and temporal resolutions between auto-correlated dataset (Efron, 1979). This was calculated with the R package 'treeclim' (Zang and Biondi, 2015). Various datasets were obtained to conduct these analyses. Monthly climate data were extracted from a $0.5 \times 0.5^\circ$ landmask corresponding to Lake Duparquet ($48.00^\circ\text{N}, -79.50^\circ\text{E}$; $48.50^\circ\text{N}, -79.00^\circ\text{E}$) using the KNMI Climate Explorer (<https://climexp.knmi.nl>; Trouet and Van Oldenborgh, 2013). Monthly gridded temperature and precipitation were obtained from 1901 to 2016 CRU TS 4.03 (Harris et al., 2020) and monthly snow-cover extent were obtained from 1966 to 2016 NOAA/NCDC Rutgers Snow cover at a $1 \times 1^\circ$ resolution (Estilow et al., 2015). Correlations were also conducted with Lake

Duparquet's observational ice-breakup dates from 1960 to 2016 (Mongrain, 2014; pers. comm. 2017) and reconstructed water levels from maximum ice-scar height associated with spring ice-breakup (Tardif and Bergeron, 1997b). Existing hydrological reconstructions from subarctic Québec were also used. Correlation coefficient between the ice-scar chronologies from Bégin (2001), Lemay and Bégin (2008) and Boucher et al. (2011) as well as the May, Spring (March–April–May) and annual discharge reconstructions respectively from Boucher et al. (2011), Nicault et al. (2014) and Nasri et al. (2020) were compared with the Harricana River spring discharge reconstruction using 40-year moving windows lagged by 21 years to assess temporal stability. Finally, we used discharge data from not only the Harricana River itself, but from nine unregulated hydrometric stations (Table 1; Water Survey of Canada, <https://wateroffice.ec.gc.ca>) with at least 25 years of records and located within a radius of 300 km of Lake Duparquet.

The impacts of several large-scale ocean-atmosphere circulation features on the variability of hydroclimate and extreme events have been documented in different parts of the world (Bush and Lemmen, 2019). For example, across North America and Canada, flooding and river ice phenology have shown to be influenced by sea surface temperature anomalies in the equatorial Pacific, i.e. phases of the El Niño Southern Oscillation (Bonsal et al., 2006; Kundzewicz et al., 2019). To further assess how large-scale atmospheric circulation indices correlated to spatial and temporal variations in reconstructed spring discharge, we included in these analyses the Atlantic Multidecadal Oscillation (AMO) from 1856 to 2016, the Arctic Oscillation (AO) from 1871 to 2011, the North-Atlantic Oscillation (NAO) from 1821 to 2016 and the reconstructed NAO (RNAO) from 1770 to 2001 downloaded from https://www.psl.noaa.gov/gcos_wgsp/Timeseries/. The El-Niño Southern Oscillation (NINO3.4) index for 1854–2016, and the Pacific Decadal Oscillation (PDO ERSSTv5) index for 1880–2016 were also downloaded from KNMI Climate Explorer (Trouet and Van Oldenborgh, 2013).

The continuous wavelet transformation (CWT) was used to decompose the variance in the spring discharge reconstruction in low and high frequencies (Torrence and Compo, 1998). The temporal variability of the reconstructions was evaluated by transforming the time series into CWT on a $\omega_0 = 6$ Morlet power spectrum base with the 'WaveletComp' package in R (Roesch and Schmidbauer, 2018). In this way the Morlet wavelet scale is comparable to the Fourier period (Torrence and Compo, 1998).

3. Results

3.1. Predictor chronology characteristics

The 12 anatomical and ring-width chronologies developed for Lake Duparquet cover 1770 to 2016 (246 years) and have an average sample length of 120 years (Fig. 2). Crossdated tree-ring series were strongly temporally coherent within the two common periods 1855–1950 and 1940–2005 (Table 2). The number of series in site chronologies exceeds 10 from 1820 to 2016, and both 40-year running windows of SSS and Rbar demonstrated the stability of the common signal through this period ($\text{SSS} \geq 0.85, \text{Rbar} \geq 0.20$; Fig. 2). The MVA and L25 chronologies showed a higher SSS than the N, pE, and TVA chronologies and an even higher SSS than the rest of the chronologies over the first 50 years (1770 to 1820; Fig. 2). To further test the stability of the common earlywood vessel signal, we recomputed successively the MVA chronology using the 5, 10, 20 and 30 longest series. For $n = 5$ series, the SSS was maintained above 0.70 for the complete 1770–2016 period (results not shown) indicating the potential to provide high-resolution reconstruction when using the 43 series available.

3.2. Reconstruction of Harricana River spring discharge

Transfer functions were successfully derived for reconstructions REC1 and REC2 (Table 3). In REC1, stepwise regression selected the first

Table 1

Hydrological stations from the Water Survey of Canada (WSC). The numbers (No.) refer to Fig. 1 and the distance is relative to Lake Duparquet. Note that the two Harricana River stations (No. 4 & 5) were combined into one for calibration purposes as there were no value differences in the overlapping period and in drainage area.

No.	Station name	Federal Id	Distance (km)	Latitude/Longitude	Drainage Area (km ²)	Period
1	downstream Kinjévis River	02JB013	30	48°22' N; 78°51' W	2590	1971–2016
2	upstream Kinjévis River	02JB003	70	48°27' N; 78°21' W	1680	1937–1965
3	Blanche River	02JC008	80	47°53' N; 79°52' W	1780	1968–2016
4	Harricana River (old gauge)	04NA002	85	48°34' N; 78°07' W	3680	1915–1933
5	Harricana River (new gauge)	04NA001	85	48°36' N; 78°06' W	3680	1933–2019
6	Porcupine River	04MD004	130	48°33' N; 81°03' W	408	1977–2015
7	Kipawa River	02JE015	155	47°04' N; 79°18' W	5980	1962–2011
8	Turgeon River	04NB001	170	49°59' N; 79°05' W	11,200	1969–1999
9	North French River	04MF001	310	51°04' N; 80°46' W	6680	1967–2016
10	downstream Missinaibi River	04LM001	310	50°35' N; 82°05' W	22,900	1973–2016
11	upstream Missinaibi River	04LJ001	320	49°36' N; 83°16' W	8570	1920–2016

(PC1, $R^2 = 63.87$), and the second principal component PC2 t_{+1} ($\Delta R^2 = 2.98$) and PC2 t_{-1} ($\Delta R^2 = 1.65$) as the best set of predictors. PC1 is driven by variables related to vessel size and number, while PC2 is driven mainly by ring-width (result not shown). Three predictors were also selected for REC2; MVA chronology ($R^2 = 61.92$), LW t_{+1} ($\Delta R^2 = 4.42$), and EW t_{-1} ($\Delta R^2 = 1.42$). In the two models, mean early-wood vessel area and number (PC1 in REC1, and MVA in REC2) account for the majority of the explained variance of Harricana spring discharge over the calibration period. The coherency between observed and reconstructed discharge was strong (Supplementary Fig. S2) and statistics were similar for the two models, whose determination coefficients (R^2) differ only slightly: 68.5% for REC1 and 67.8% for REC2 (Table 3).

In both models, the cross calibration-verification exercises for the two periods (1915–1965 and 1966–2016) indicated considerable predictive skill (Table 3; Fig. 3a) and approximately normally distributed residuals. The range of reconstructed discharge (73 to 184 m³/s) remains within that of the observed values (63 to 196 m³/s) and the reconstruction errors expressed in the units of observed discharge (MAE) are small and similar for both models (12.0 m³/s). The verification statistics RE and CE are strongly positive suggesting that low and high frequencies were very well reproduced by the two reconstructions (Table 3). The year-to-year direction and amplitude in discharge are also well reproduced (Fig. 3a), as indicated by the significant sign tests and product-mean test (PMT) (Table 3).

The strength of the common signal and the temporal stability of the reconstructions during the period of juvenile growth were assessed by recalculating the models using the first 50 years of each tree-ring width and anatomical series. Since sample replication decreases over time and the growth rate is maximal in young trees, the noise in these parts of chronology may be considered maximal. REC1 from a model limited to the first 50 years of the series spans 1770–2004 and is strongly associated with REC1 from the full data ($r = 0.884$, $p < 0.001$, $n = 231$). The restricted REC1 model performs well, with statistics adjR² = 49.3, F = 44.20 and MAE = 14.98 m³/s comparable to those of the full REC1 model. Similar stability was observed for the REC2 model (result not shown). Given the similarities between both models ($r = 0.96$, $p < 0.001$, $n = 246$), the REC1 based on the full data was used for the remaining analyses.

3.3. Extreme low and high discharge

To assess whether reconstruction (REC1) accuracy differs in years of high vs low spring discharge (Fig. 3a), thresholds at the mean ± 1.5 sd were calculated from the instrumental Harricana spring discharge, 1915–2016 (high value = 159.8 m³/s, low value = 80.3 m³/s). Over the calibration period, high discharge years were 1922, 1928, 1933, 1947, 1960, 1967, 1974 and 1979 (2019 also but outside the calibration period). Low discharge years were 1931, 1963, 1998, 2003, 2010 and 2012 with the four lowest discharge values from 1915 to 2016 recorded after 1998 (Fig. 3a). For the eight highest and six lowest discharge years,

the MAE of the reconstruction were comparable, being respectively 18.7 m³/s \pm 11.3 and 23.8 m³/s \pm 6.4.

The reconstruction's ability to capture the variability of the Harricana River flood regimes was determined by calculating a K-Means clustering of the daily Harricana River hydrograph from April 15 to June 30 for years 1915–2020 to identify conditions leading to low and high spring discharge (Fig. 3b). Four clusters were identified: 1) late break-up with maximum spring discharge, 2) late break-up with low spring discharge, 3) early break-up with minimum spring discharge and 4) early break-up with intermediate spring discharge (Fig. 3b). The eight highest discharge years identified in the calibration data (Fig. 3a) were evenly distributed between cluster 1 ($n = 4$) and 4 ($n = 4$), and the six lowest discharge years corresponded to cluster 3. Interestingly, the clusters associated with early break-up with minimum to intermediate discharge (cluster 4 and mainly cluster 3) have dominated since about 1998 to 2012. Comparison of the mean errors (instrumental discharge minus REC1 values) and standard deviation corresponding to each cluster indicates that clusters 1 and 4 are slightly underestimated and cluster 3 is slightly overestimated in REC1 model (cluster 1: 9.97 \pm 16.27, cluster 2: -1.74 ± 13.92 , cluster 3: -9.60 ± 11.52 , cluster 4: 7.27 ± 13.96). This suggests that REC1 is robust in reconstructing both the timing and magnitude of spring discharge and performs equally well for both low and high discharge. It should be reemphasized that the difference between low and high extremes may have intensified in the last 20 years of the reconstruction (1997–2016) with more frequent low and intermediate levels (cluster 3 = 10/20 years and cluster 4 = 7/20 years; Fig. 3a). During this period, the low discharge years were less well captured by the reconstruction model.

3.4. Temporal stability in the spring flood reconstruction

Three distinct periods can be observed in REC1 as highlighted by both the 10-year smoothing spline (Fig. 4a) and the CWT analysis (Fig. 4b). A first period from about 1771 to 1850 shows a low-frequency multi-decadal variability (Fig. 4a) and a wavelet power spectrum with a persistent and significant high variance close to a periodicity of 32 years (Fig. 4b). A second period is observed from ~1850 to 1950 and shows a decadal variability at low frequency (Fig. 4a) in which the variance is high and significant near a periodicity of 26 years but mixed with smaller patches with periodicities of 4 to 8 years (Fig. 4a). A third period from ~1950 to 2016, shows a low-frequency variability that may return to multi-decadal frequencies (Fig. 4a), with however significant high variance patches between 2 and 4-year periodicity bands (Fig. 4b).

The evolution of spring discharge periodicity between these three periods suggest a change in the recent variability toward a higher frequency of high spring discharge after the Little Ice Age (1850–1870 CE; Matthews and Briffa, 2005; Fig. 4). The majority of high discharge years were recorded after the end of Little Ice Age and the highest discharge after 1950 (1960 and 1979). The majority of the low discharge were also recorded between 1850 and 1950, but the extreme minima were in

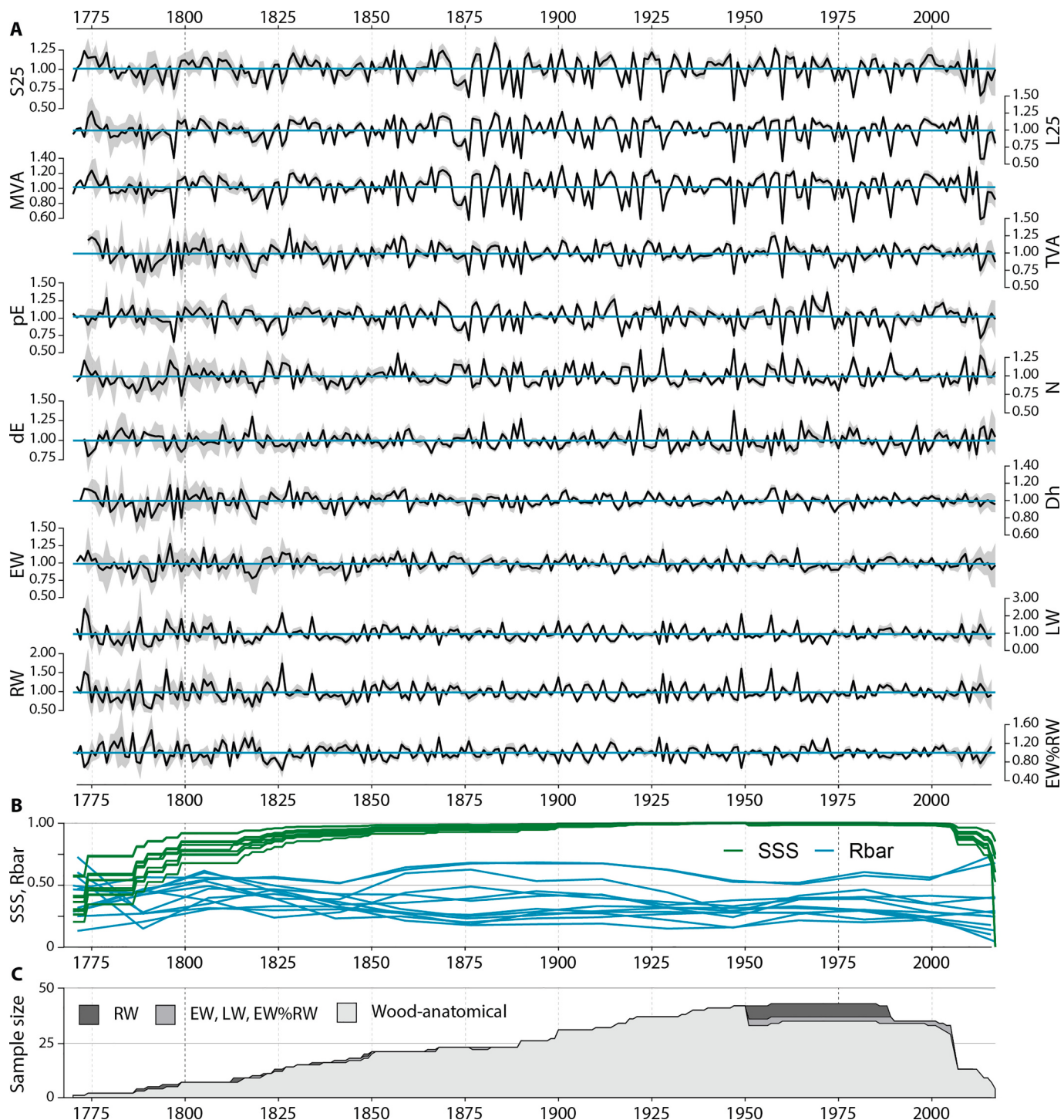


Fig. 2. Chronology characteristics. A) Tree-ring anatomical and width chronologies developed for Lake Duparquet. Abbreviations of chronologies are listed in Table 2. The grey shade indicates the two-standard-error confidence intervals. B) 30-year running windows of subsample signal strength (SSS, green) and mean inter-series correlation (Rbar, blue). C) Yearly sample size for ring-width and anatomical chronologies expressed as number of trees per year. (For interpretation of the references to colour in this figure legend, the reader is referred to the web version of this article.)

1775, 1901 and 1958 (Fig. 4). It should be remembered however, that the last low discharge events (1996–2016) were less well captured by REC1 model.

Using a linear regression of the 30 highest and 30 lowest values from REC1 over the period 1771–2016, the increase in spring maximum discharge can be quantified as $1 \text{ m}^3/\text{s}$ per decade ($R^2 = 0.334, p < 0.001$; Supplementary Fig. S3). No linear trends were revealed in mean and in the 30 lowest values from REC1 spring discharge: the R^2 coefficients are

close to zero (Supplementary Fig. S3). In addition, the mean discharge calculated over the three periods identified in the CWT (1771–1850; 1850–1950; 1950–2016) remained very stable ($sd = 0.82 \text{ m}^3/\text{s}$). However, using a linear regression of the 10 lowest values from Harricana River instrumental spring discharge from 1915 to 2016, a trend toward a decrease in spring minimum discharge is revealed ($R^2 = 0.363, p < 0.001$; results not shown).

Table 2Descriptive statistics of the 12 anatomical and ring-width chronologies derived from 43 *Fraxinus nigra* trees sampled at Lake Duparquet.

Chronologies ^a	Type ^b	1st Common period 1855–1950			2nd Common period 1940–2005		
		Variance explained by the first eigenvector (%)	Rbar ^c	N° of series	Variance explained by the first eigenvector (%)	Rbar ^c	N° of series
L25	S	70.83	0.64	20	70.54	0.57	27
S25	S	48.21	0.43	20	38.45	0.33	27
MVA	S	72.03	0.65	20	70.44	0.57	27
TVA	R	44.25	0.39	20	44.32	0.36	27
pE	S	59.52	0.54	20	44.94	0.38	27
N	R	48.50	0.40	20	49.14	0.41	27
dE	R	41.70	0.32	20	34.04	0.27	27
Dh	R	30.70	0.25	20	33.04	0.26	27
EW	R	25.77	0.20	21	28.03	0.22	31
LW	R	35.86	0.29	21	36.53	0.28	31
RW	R	37.69	0.31	21	38.40	0.30	31
EW%RW	R	30.76	0.25	21	32.25	0.25	31

^a Abbreviations of chronologies are as follows: (L25 and S25) mean lumen cross-sectional area of the 25% largest (L) and smallest (S) earlywood vessels, (MVA) mean and (TVA) total earlywood vessel lumen cross-sectional area, (pE) porosity within the earlywood, (N) number of earlywood vessels, (dE) density of earlywood vessels, (Dh) hydraulic diameter, (EW) earlywood width, (LW) latewood width, (RW) total ring width, (EW%RW) proportion of earlywood within the total ring width.

^b Depending on autocorrelation significance, standard (S) or residual (R) chronologies were selected for analysis.

^c Inter-tree correlation coefficient (Rbar) computed for the two common periods.

Table 3

Statistics for the split-sampling calibration and verification procedure, and the full period reconstruction. Models REC1 and REC2 are presented together.

Calibration	MODEL REC1: PCA reduced series			MODEL REC2: non-reduced series		
	1915–2016	1915–1965	1966–2016	1915–2016	1915–1965	1966–2016
R ²	0.685	0.748	0.670	0.678	0.752	0.647
Adjusted R ²	0.675	0.732	0.649	0.668	0.736	0.624
Standard Error (SE) of the estimate	15.060	14.490	14.820	15.240	14.370	15.320
F-statistic	71.040	46.400	31.750	68.648	47.421	28.677
p-value	<0.001	<0.001	<0.001	<0.001	<0.001	<0.001
Verification	1915–2016	1966–2016	1915–1965	1915–2016	1966–2016	1915–1965
Pearson correlation coefficient r	0.828	0.817	0.788	0.823	0.827	0.782
p-value	<0.001	<0.001	<0.001	<0.001	<0.001	<0.001
Root Mean Squared Error (RMSE)	14.761	16.379	17.569	14.935	13.795	14.710
Mean Absolute Error (MAE) in m/s	11.936	13.083	14.023	12.012	14.152	16.251
Reduction of Error (RE)	0.685	0.569	0.602	0.678	0.538	0.477
Coefficient of Efficiency (CE)	/	0.562	0.597	/	0.531	0.471
Product-mean test (PMT) (on z-scores)	5.331	3.942	3.143	5.396	3.725	3.417
Sign tests (on z-scores)						
Agreements	86	41	45	82	42	44
Disagreements	16	10	6	20	9	7

3.5. Reconstructed spring discharge, climate, ice-breakup and large-scale atmospheric circulation indices

REC1 spring discharge was significantly correlated with climate conditions leading to maximum spring discharge (Fig. 5). Field correlations indicated a strong and positive association between spring discharge and April and May snow cover across much of central/eastern north Canada with most significant contour encompassing the study area, most of Ontario and eastern Manitoba (Fig. 5a). Low temperature and abundant precipitation in the previous December, during ice freeze-up, were positively and significantly associated to spring discharge (Fig. 5b). Similarly, both temperature and precipitation in spring (March and April) were respectively negatively and positively associated with spring discharge (Fig. 5b). Maximum spring discharge thus tended to occur during years with an early, cold winter, late spring and thick winter snowpack. Interestingly both reconstructed and instrumental spring discharge were also significantly and positively associated with observed ice-breakup dates for Lake Duparquet over the period 1968–2016 (REC1: $r = 0.493$, $p < 0.001$; Harricana instrumental: $r = 0.346$, $p < 0.001$), indicating that in the latest portion of the 20th century, maximum flooding tended to occur in years with a late ice-breakup.

Correlations of reconstructed discharge (REC1) with large-scale

atmospheric circulation indices for the common period 1880–2016 revealed seasonal negative and positive associations (Fig. 5c). Discharge was significantly negatively correlated with January to May NINO3.4 and March to May AMO. For both indices, correlation was strongest in April (April NINO3.4, $r = -0.20$; April AMO, $r = -0.22$; $p < 0.001$). Significant positive associations also occurred in summer with June AO ($r = 0.16$, $p < 0.05$) and May to July NAO, with the highest NAO correlation in July (July NAO, $r = 0.30$, $p < 0.001$). The association was not significant with PDO in spring or summer PDO but was significant in previous September ($r = -0.14$, $p < 0.05$).

3.6. Spatial agreement between REC1 and hydrological data and dendrohydrological reconstructions at the regional level

REC1 spring discharge is strongly coherent with regional hydrological gauge data over the second half of the 20th century (Table 4). Correlations with REC1 tended to decrease with distance from Lake Duparquet. The highest correlation was observed with the ‘upstream Kinojévis River’ gauge ($r = 0.92$, $n = 29$, $p < 0.001$) and the lowest correlation with the ‘Northern French River’ ($r = 0.52$, $n = 50$, $p < 0.001$), representative respectively of the closest and the farthest from the hydrological stations (Table 4).

Reconstructed spring discharge of the Harricana River shares

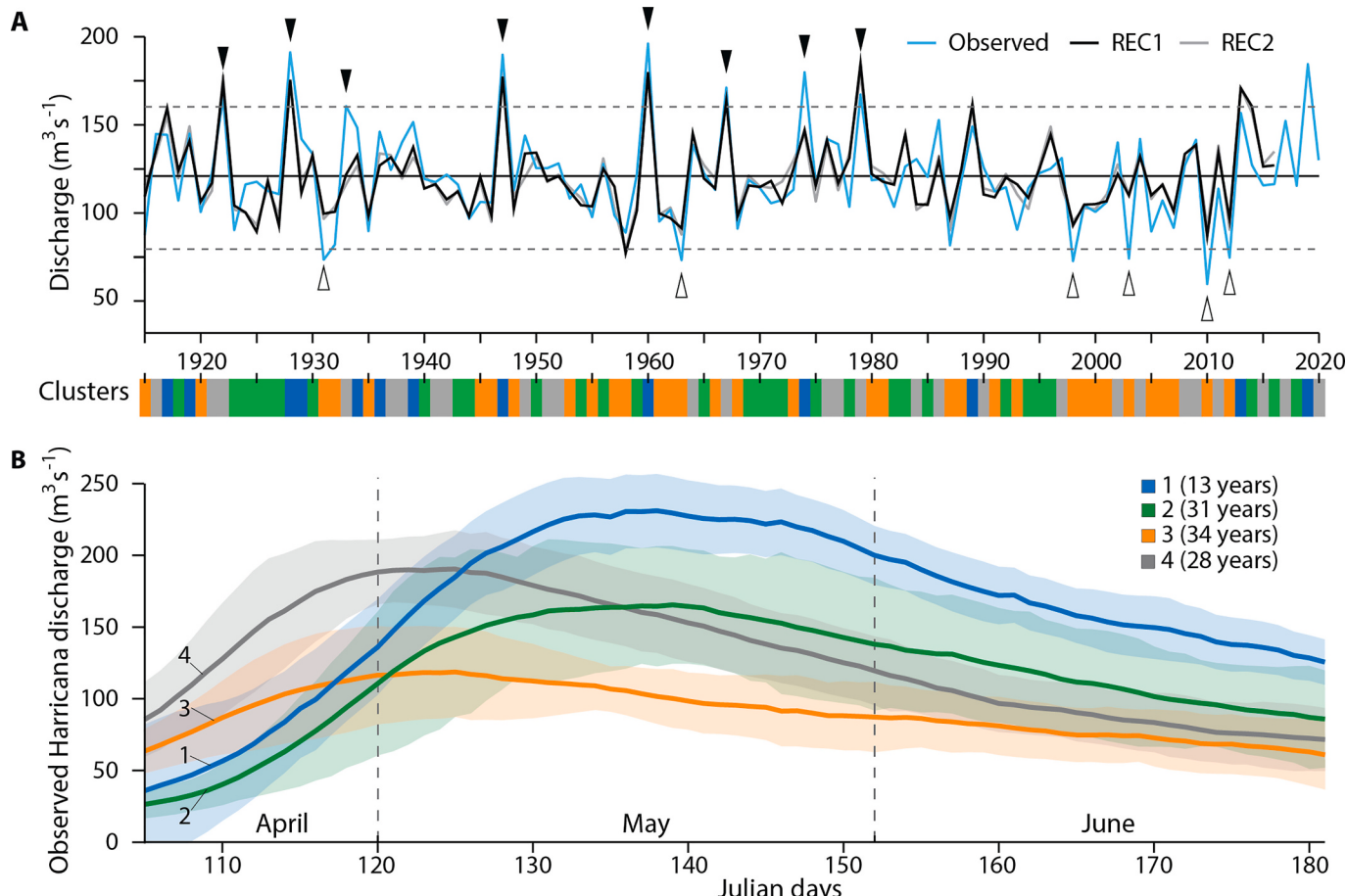


Fig. 3. Comparison between observed and reconstructed discharge. A) Instrumental (blue) and reconstructed Harricana River spring discharge for the two models REC1 (black) and REC2 (grey) for the 1915–2016 calibration period. Horizontal lines mark the mean (solid) and $\pm 1.5 \text{ sd}$ (dashed) of the instrumental Harricana spring discharge. High (black triangles) and low (white triangles) discharge years exceed the threshold $\pm 1.5 \text{ sd}$. B) The four K-Means clusters of daily instrumental Harricana spring discharge from April 15 to June 30 and from 1915 to 2020. Shaded areas indicate standard deviation within each cluster. The number in parenthesis represents the number of years in each cluster. (For interpretation of the references to colour in this figure legend, the reader is referred to the web version of this article.)

features with other hydrological reconstructions from tree-rings and ice-scar chronologies developed for boreal and subarctic Québec (Fig. 6). REC1 was positively and significantly correlated with the ice-scar chronology developed for Lake Duparquet for the period 1850 to 1989 ($r = 0.434$; $p < 0.001$) and in each of the 40-year moving windows lagged by 21 years over that period (Fig. 6). This suggests that ice scars were more numerous during years of high reconstructed spring discharge. Correlations of REC1 with other proxies in a 40-year moving window were less temporally coherent but reveal several positive associations since the 20th century. The ice-scar chronologies from Corvette Lake, Lake Bienville and the reconstruction of the May discharge of the Caniapiscau Reservoir were positively correlated with REC1, but the p -value exceeds 0.05 (Fig. 6).

The ice-scar chronologies showed a gradient of intensification of spring ice scarring activity over time, with visible changes in magnitude around the 1870s and 1930s (Fig. 6). The ice-scar chronology from Lake Duparquet and the discharge reconstructions from Caniapiscau Reservoir (May, spring and annual) also share the periods of low discharge (1825) and high discharge (1875, 1970) but not the persistent drought period of the early 1900s, illustrated mainly in the reconstructed spring discharge of the Caniapiscau Reservoir (Fig. 6). Moving correlation windows (40 years) also show a change in sign of associations between REC1 and the rest of subarctic Québec over time. The correlations were predominantly negative until 1850 and changed to predominantly positive correlations in 1990, with the exception of Lake Montausier.

4. Discussion

4.1. Strength of the Harricana spring discharge reconstruction

This work provides a unique annually resolved multi-century reconstruction of spring discharge and paleofloods for the Canadian northeastern boreal region. The performance statistics of the reconstruction are comparable to some of the most accurate tree-ring reconstructions of river discharge (Meko and Graybill, 1995; Woodhouse et al., 2006; Boucher et al., 2011). This study highlights the potential of using riparian trees as hydrological proxies and demonstrates the value of anatomical variability in tree rings to reconstruct low and high spring discharge with comparable accuracy. The greatest potential has been demonstrated with continuous measurements of the cross-sectional area of earlywood vessels (MVA) and number of earlywood vessels (N), and particularly with the MVA chronology, which is itself a proxy for spring discharge of the Harricana River. The juvenile tree growth in the total chronologies or the sample size in the first part of the chronologies were found to have a very limited influence on the common signal. Other anatomical and ring-width variables used as predictors of spring discharge (S25, L25, TVA, pE, dE, Dh, EW, LW, RW, EW%RW) showed less or no association to the spring discharge.

A recurring difficulty in dendrochronological reconstruction of river discharge is to capture adequately both high and low discharge. Most hydrological reconstructions have been derived from precipitation-

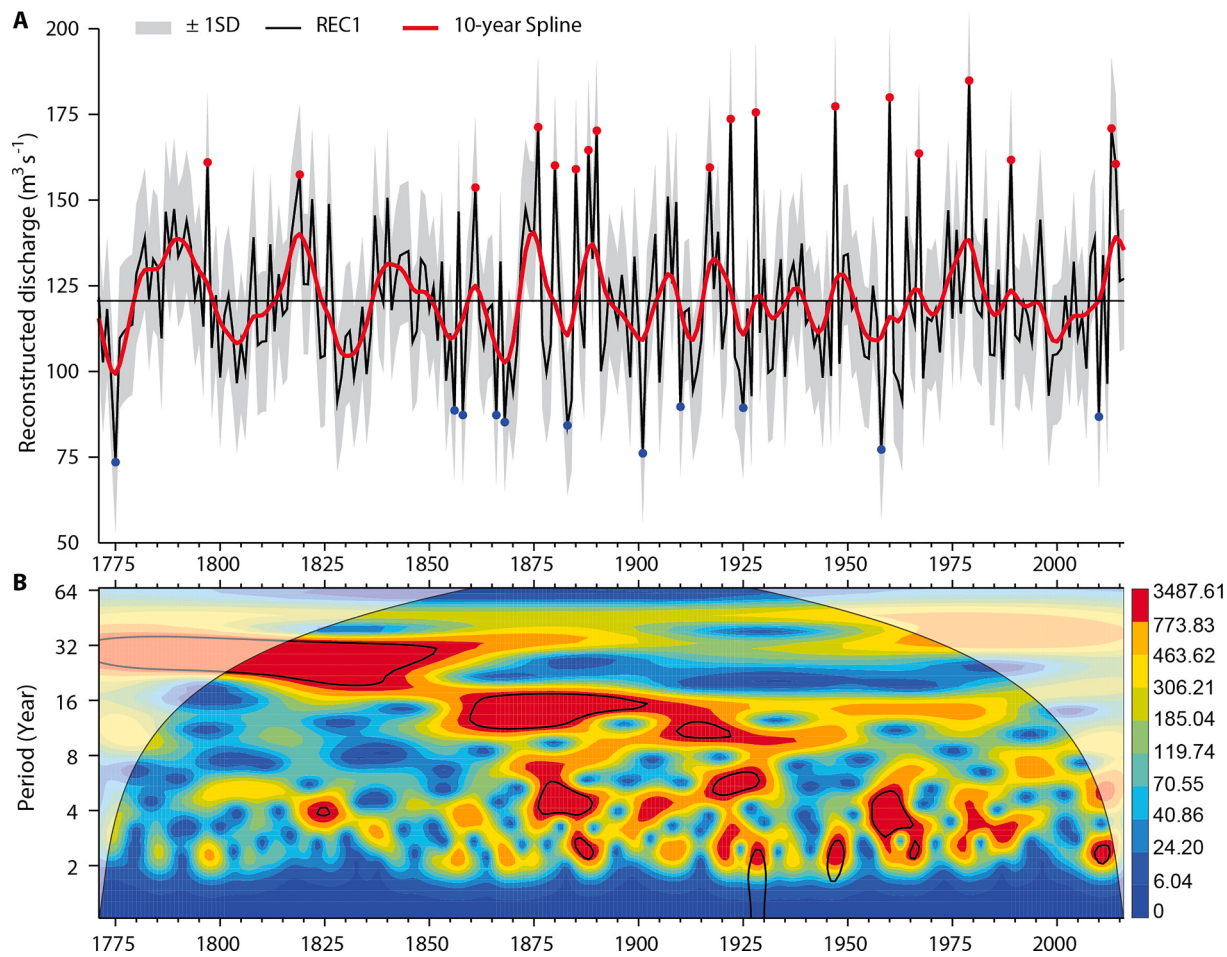


Fig. 4. Reconstruction characteristics. A) Reconstruction of Harricana River spring discharge (April 15 to June 30) from 1771 to 2016. Decadal variations are highlighted by a 10-year smoothing spline (red curve) and confidence intervals correspond to the standard deviation envelope ($\text{sd} = 20.49 \text{ m}^3/\text{s}$; grey shade). High (red dots) and low (blue dots) discharge years exceed the threshold of the mean $\pm 1.5 \text{ sd}$. Horizontal line at $120.60 \text{ m}^3/\text{s}$ marks the mean for the 1771 to 2016 period. B) Decomposition of REC into Morlet 6th power in continuous wavelet transformation. The black lines encircle areas were $p < 0.05$, tested against white noise background as lag-1 autocorrelation in REC1 was not significant. The white shaded area indicates the cone of influence where wavelets are stretched beyond the range of reconstructed data and may be altered by edge-effects. Variance magnitude range for blue (low) to red (high). (For interpretation of the references to colour in this figure legend, the reader is referred to the web version of this article.)

sensitive trees growing in semi-arid environments (Meko et al., 2001; Woodhouse et al., 2006; Biondi and Meko, 2019; Martínez-Sifuentes et al., 2020) while few have used trees growing directly on floodplains (Agafonov et al., 2016; Meko et al., 2020). In arid environments, the difficulty lies in capturing high discharge given that sites and trees are sampled to maximize drought (low discharge) signal. Also, because flooding is linked to heavy rainfall, which can result in moisture no longer being the limiting factor to growth, tree-ring width of drought-sensitive trees is not a good indicator of variations in high levels of flooding (Meko and Graybill, 1995). In boreal environments, where high discharge is mostly associated with spring thaw (Aygün et al., 2019), reconstructions of spring discharge using trees from uplands have shown that tree-ring width may not record years of high spring discharge when thaw occurs before the beginning of the growing season (Nicault et al., 2014). Indeed, the variability of the latewood width in a given year is generally higher than that of the earlywood and may negatively influence the earlywood width in the following year (Tardif, 1996; Tardif and Conciatori, 2006), which explains why early, late, and total tree-ring widths may not capture the full range of hydrological variability (Kames et al., 2016).

The use of ring-porous trees growing in flood-prone environments and their anatomical response to annual floods has demonstrated the usefulness of flood rings in dendrohydrology (St. George and Nielsen,

2000; St. George and Nielsen, 2003; Therrell and Bialecki, 2015; Kames et al., 2016; Meko and Therrell, 2020). More broadly, in environments where the period of flooding is sufficiently long and overlaps the period of formation of earlywood vessels in submerged stem portions, flood rings can be used to identify historical flood years. In addition, year-to-year measurements of earlywood vessel characteristics can extend hydrological records by reconstructing a wider hydrological spectrum i.e., from low to high discharge years.

4.2. Spatial coherency of spring discharge and flooding

Positive and highly significant correlations between REC1 and that of the nine surrounding hydrological stations compared well with the results of Kames et al. (2016). In addition, the similarities shared with other published paleorecords of spring flooding from sub-arctic Québec support a strong common hydrological signal across the study area and for the early 20th to early 21st centuries. In their analysis of spring flood duration and frequency, Javelle et al. (2003) identified our study area as part of a large homogeneous region from central Ontario to southwestern Québec, mainly explained by the distribution of maximum snow depth between 1980 and 1995. When developing the regional flood equations for Ontario and Québec, Gingras et al. (1994) had already suggested a similar region around our study area where most of the

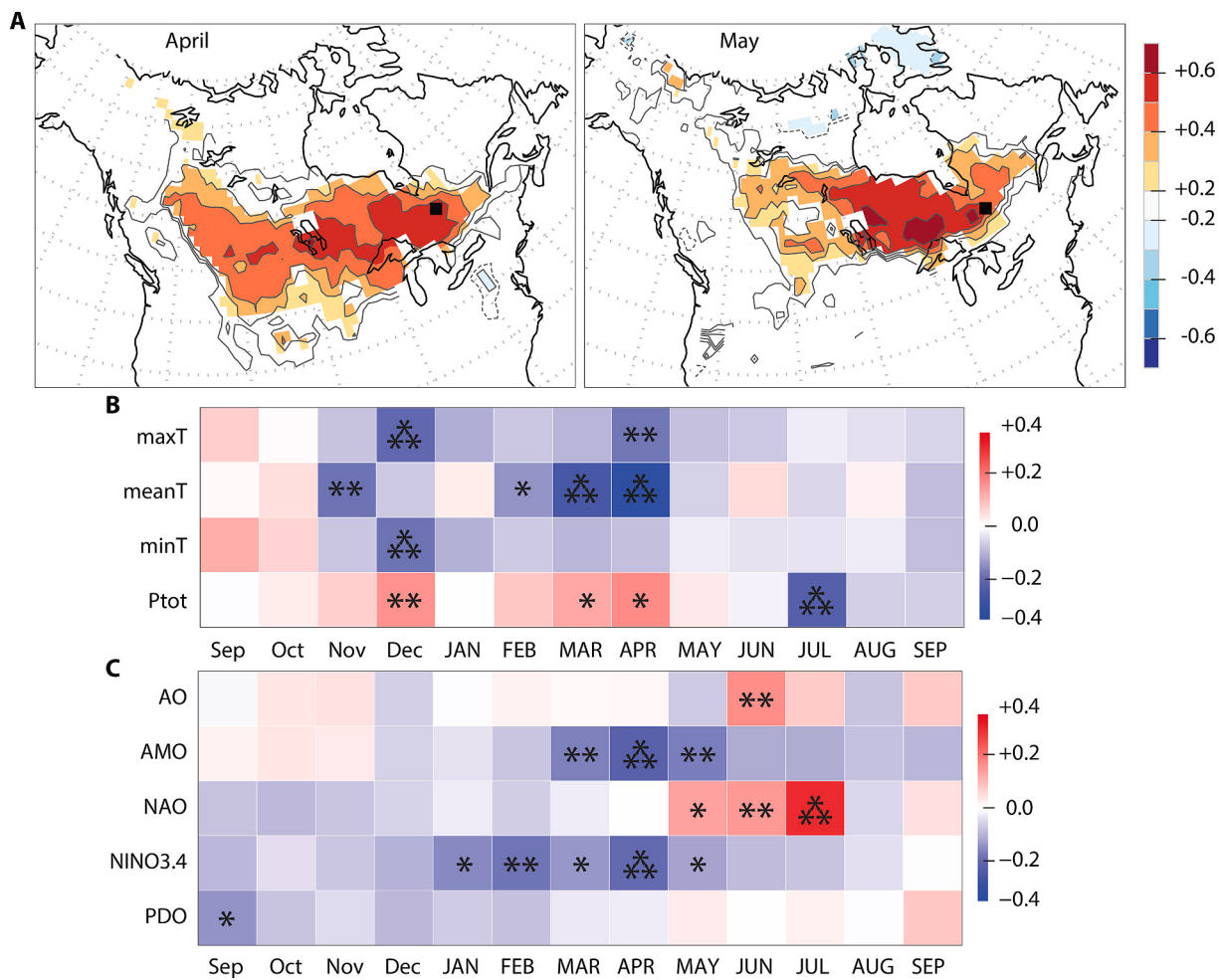


Fig. 5. Climate signals. A) Spatial correlations ($p < 0.1$) between REC1 and April and May (1966–2016 NOAA Rutgers snow cover). The black square indicates Lake Duparquet location. B) Bootstrapped correlation coefficients between REC1 and monthly maximum, mean, minimum temperature (maxT, meanT, minT) and total precipitation (Ptot) (1901–2016 CRU TS 4.03). C) Bootstrapped correlation coefficients between REC1 and large-scale atmospheric circulation indices for the common period 1880–2016. Correlation coefficients in A, B and C panels range from red (positive correlation) to blue (negative correlation). Asterisks in B and C panels indicate p -value <0.1 (*), <0.05 (**), and <0.01 (***) (For interpretation of the references to colour in this figure legend, the reader is referred to the web version of this article.)

flooding was generated by snowmelt from April to June.

While no latitudinal or longitudinal gradient in the strength of the associations between REC1 and hydrological stations was observed, regional differences can be distinguished between Lake Duparquet and subarctic Québec (to the north), the Great Lakes (to the south), Ontario and Manitoba (to the west of the study area). For example, the exceptional spring flood years recorded regionally were not always identical among regions, but some floods years were common across eastern Canada: the 1979 flood occurred in Manitoba, Ontario, Québec and New Brunswick after intense rainfall combined with heavy snowmelt late in the spring (Payette, 1980; Tardif and Bergeron, 1997b; Burton, 2015); the 2017 spring flood affected the province of Québec (Davies, 2017); and the more intense spring flood of 2019 affected Ontario and the Great Lakes, Québec, and New Brunswick (Bilefsky and Austen, 2019; McNeil, 2019; Turcotte et al., 2019). However, the return frequency of spring floods over the last 250 years appears to be higher in the study area than in Manitoba, for instance, where 10 floods were recorded on the Red River for the period 1750–1999 (St. George and Nielsen, 2003) compared to 26 floods reconstructed from 1770 to 2016 on the Harricana River.

At low frequencies, the long-term changes observed in REC1 are also consistent with changes identified in an ice-scar chronology from Lake Duparquet (Tardif and Bergeron, 1997b) and to changes observed in

subarctic Québec, where periods of low discharge (1820–1850; 1920–1950) and high discharge (1870–1920) are associated with an increase in lake levels and glacial activity (frequency and maximum height of ice scars) since the 1850s and even more so since the 1950s (Tardif and Bergeron, 1997b; Bégin, 2000; Bégin, 2001; Lemay and Bégin, 2008; Boucher et al., 2011; Nicault et al., 2014; Nasri et al., 2020). Multi-century ice-scar chronologies from northern Québec share similar upward trends in spring flooding over the 20th century with REC1, although there are some regional contrasts. Multi-proxy reconstructions of spring discharge for the Caniapiscau reservoir (Boucher et al., 2011; Nicault et al., 2014; Brigode et al., 2016) also showed higher and more variable levels since 1965. In boreal Lake Duparquet, an increase in the frequency and magnitude of ice scarring was observed since the end of the Little Ice Age (LIA; 1850–1870 CE; Matthews and Briffa, 2005) with a peak increase in the 1930s followed by continued high ice scarring activity (Tardif and Bergeron, 1997b). Major spring flood years were also visible in these ice-scar chronologies, particularly in 1947, 1960 and 1979 (Tardif and Bergeron, 1997b; Lemay and Bégin, 2008). Recruitment of *F. nigra* (Tardif and Bergeron, 1999) and *Thuja occidentalis* (Denneler et al., 2008) trees on the shores of Lake Duparquet has also been shown to be reduced along the shorelines relative to higher elevations, in response to the increased frequency of flooding and ice scarring since the 19th century that has increased the exposure of

Table 4

Pearson correlation coefficients between reconstructed Harricana River spring discharge from April 15 to June 30 (REC1) and mean instrumental discharge from April 15 to June 30 at nine hydrometric stations surrounding Harricana River and Lake Duparquet. The table is ordered by distance to Lake Duparquet (top to bottom). Each correlation in bold corresponds to p -value <0.001 . Note that the periods and number of years differ between hydrometric stations.

No	Station	Id	Period	N years	Distance (km)	REC1
1	downstream Kinojévis River	02JB013	1971–2016	46	30	0.86
2	upstream Kinojévis River	02JB003	1937–1965	29	70	0.91
3	Blanche River	02JC008	1968–2016	49	80	0.76
4,5	Harricana River 2	04NA001-2	1915–2016	102	85	0.82
6	Porcupine River	04MD004	1977–2015	26	130	0.80
7	Kipawa River	02JE015	1962–2011	39	155	0.56
8	Turgeon River	04NB001	1969–1999	27	170	0.74
9	North French River	04MF001	1967–2016	50	310	0.52
10	downstream Missinaibi River	04LM001	1973–2016	43	310	0.69
11	upstream Missinaibi River	04LJ001	1920–2016	97	320	0.57

riparian stands.

Despite the similarities (positive correlations) between REC1 and ice-scar chronologies from Lake Duparquet and subarctic Québec, these records do not always match and may represent regional differences and/or fundamental differences in the nature of the proxies used. For example, ice scars reflect mainly lake-ice phenology and ice-push abrasion while flood rings mainly reflect the persistence of flooding and anoxia. Tardif and Bergeron (1997b) suggested that records of ice scars on lakes may not adequately reflect flood levels on rivers. Lakes in the Abitibi region freeze earlier and thaw later than rivers, and lake ice is also thicker and less mobile than on rivers where the current is stronger. In addition, the accumulation of shore ice, the timing between the thaw and the maximum water level, or complex differences of ice regime and decay between sites are also known to affect the relationship between flood water levels and the height and frequency of ice-scars (Tardif and Bergeron, 1997b; Lemay and Bégin, 2008; Boucher et al., 2011; Liedensschmidt et al., 2018). Ice-scar formation are also reflective of specific conditions (e.g., daily winds, lake morphology) occurring over a short temporal window associated with ice break-up (Tardif and Bergeron, 1997b; Lemay and Bégin, 2008) whereas flood rings integrate hydro-climate conditions occurring over a larger temporal window and including post ice break-up events like spring precipitation leading to prolonged flooding. Ice scars are also recorded at a time trees are dormant whereas flood rings and year-to-year changes in earlywood vessels reflects conditions leading to long lasting submersion of the stem during active radial growth.

Results strongly suggest that since 1770 the spring discharge dynamics in northeastern Ontario and northwestern Québec has undergone changes. While mean discharge in REC1 remained the same over the 1771 to 2016 period, changes were observed in the frequency of low to high discharge events through time. Even though reconstructed Harricana River spring discharge shows little year-to-year association with discharge records from the subarctic Québec, the comparison of datasets allows us to identify 1870 and the 1930s as breakpoints in the magnitude of spring-discharge increase. Evidence supporting a major climate shift at the end of the LIA also comes from independent data on fire cycles in the Lake Duparquet region. In eastern boreal Canada and since the end of the LIA, a pronounced decrease in the frequency and

magnitude of forest fires has been linked to a decrease in the frequency of droughts and to an increase in precipitation (Bergeron and Archambault, 1993; Drobyshev et al., 2017). Bergeron et al. (2001) also support the idea that differences in forest fire frequencies and area burned between northeastern Ontario and central Québec may be driven by climatic changes since the end of the LIA.

4.3. Spring discharge, flooding and climatic changes

While there have been no consistent trends in flooding events for Canada as a whole (Aygün et al., 2019; Bush and Lemmen, 2019), century-long discharge data records from nival regime catchments in northern Ontario support our findings by showing an increasing trend in the average magnitude of spring snowmelt floods since 1916 (Burn and Whitfield, 2018). Trend toward earlier timing of spring break-up and flooding during the 19th and early-20th centuries has however been reported in discharge records across Canada (Vincent et al., 2018; Bonsal et al., 2006), northern Ontario (Fu and Yao, 2015; Burn and Whitfield, 2018) and the Great Lakes (Jensen et al., 2007). The 20th century flood regime is shown to be affected by faster snowmelt and more intense and frequent rain and rain-on-snow events (Bush and Lemmen, 2019). However, our results suggest the contrary or at least no trend as indicated by the positive correlation found between REC1 and snow-cover extent and a negative correlation with spring maximum temperature. No seasonality change has been found either in Harricana River instrumental records since 1915 or in tree-ring based chronologies of subarctic Québec (Boucher et al., 2011). Regarding the low spring discharge levels, our reconstruction has not perfectly captured the low discharge years recorded on the Harricana River between 1996 and 2016. This period may constitute a unique period of relatively low discharge and ending in 2012, as indicated by the recurrence of major flood in 2013, 2014, 2017, and 2019. The addition of precipitation-sensitive tree-ring proxies could be beneficial for capturing additional variance associated with the increase of spring water deficit and late summer droughts (Griffin et al., 2011) documented since the end of the LIA (Girardin et al., 2006).

In this study, recent fluctuations in REC1 were associated with long winters with significant snow cover and intense spring precipitation that promotes rapid melting, especially in late spring, over much of central-east Canada. The increase in Harricana River spring mean discharge since the end of the LIA is also consistent with recorded increases in snow water equivalent, maximum snow depth in Canada (Zhao et al., 2013), and the duration of snow cover in northern Québec (Brown, 2010) since 1950. Although the influence of ENSO (and PDO) on snow cover variability in Québec has been limited in the mid to late-19th century (Bonsal et al., 2001; Bonsal et al., 2006), its influence during the 20th century has increased unprecedentedly compared to the last seven centuries (Li et al., 2013). The particularly significant associations of ENSO with monthly discharge in southern Ontario and Québec beginning in the 1960s (Nalley et al., 2012) also support the hypothesis that the increase in Harricana River maximum spring discharge could be driven by the increasing influence of ENSO.

Our reconstruction showed that the phase of NINO3.4 may influence the type and the timing of high discharge in the Harricana River. Warm, moist air masses in the equatorial Pacific Ocean (warm phase, El-Niño) may be associated with early springs and minor flooding, whereas cold, dry air masses (cold phase, La Niña) may correlate with late thaw and maximum spring discharge. This is consistent with ENSO influence on inter-annual flood variability across North America. Flooding is influenced differently during El Niño, which is associated with extreme-precipitation floods than during La Niña, which is associated with snowmelt floods (Gurrapu et al., 2016; Kundzewicz et al., 2019). There is also evidence that ENSO has strongly influenced river ice phenology (freeze-up and break-up timing, duration of river ice-period) since 1850 in Québec (Bonsal et al., 2001; Bonsal et al., 2006) and that the phase and magnitude of the PDO index modulate the impact of ENSO on winter

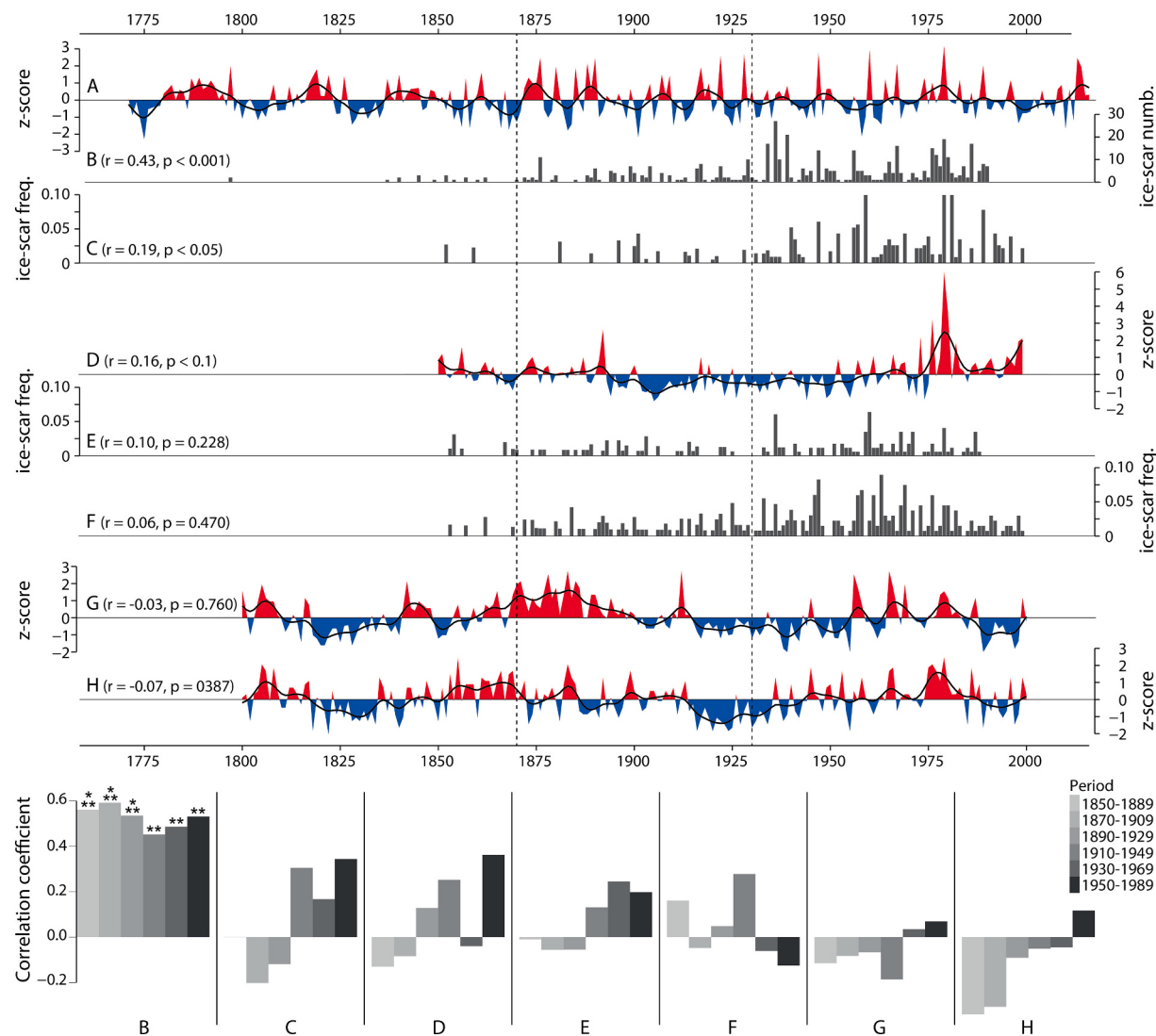


Fig. 6. Comparison of ice-scar chronologies and reconstructed spring discharge from Northern Québec. Chronologies are presented in order of decreasing correlation with (A) Harricana River reconstructed spring discharge (REC1). Other chronologies are as follows: ice-scar frequencies of (B) Lake Duparquet (Tardif and Bergeron, 1997b), (C) Corvette Lake (Lemay and Bégin, 2008), (E) Bienville Lake (Bégin, 2001), (F) Montausier Lake (Boucher et al., 2011) and reconstructions of Caniapiscau reservoir (D) May discharge (Boucher et al., 2011), (G) annual discharge (Nasri et al., 2020), and (H) spring (March – April – May) discharge (Nicault et al., 2014). Ice-scar chronologies are presented in bar plot while discharge reconstructions are presented in positive (red) and negative (blue) area with a 10-years spline. Scales are the same between reconstructions, and between ice-scar chronologies. The bottom panel presents Pearson correlation coefficients calculated in 40-year moving windows lagged by 21 years between REC1 (A) and the above-described tree-ring proxies (B to H) with asterisks indicating p -value <0.05 (*), <0.01 (**), and <0.001 (***) (For interpretation of the references to colour in this figure legend, the reader is referred to the web version of this article.)

air temperature in the Great Lakes region (Rodionov and Assel, 2003). This influences the storage of ice and snow in winter, which can then feed the spring thaw floods.

In contrast to the reconstruction of spring discharge in the Harricana River, where the AO and NAO indices may be associated with discharge conditions in summer only, spring snowmelt floods have been mainly associated with these indices in northeastern Québec (Boucher et al., 2011; Nicault et al., 2014; Brigode et al., 2016). Although NAO and AO had a limited influence on river ice phenology in Canada in the mid-19th century (Bonsal et al., 2001; Bonsal et al., 2006), their negative phases influenced the climatic conditions of previous winters and springs in northeastern Québec (Boucher et al., 2011; Nicault et al., 2014; Brigode et al., 2016). The AMO phase has also been associated with the multi-decadal magnitude of flooding across Canada (Burn and Whitfield, 2017) and been reported to modulate the relationship between the NAO and ENSO indices, particularly in late winter (Zhang et al., 2019). Across the North Atlantic Basin, Ballesteros-Cánovas et al. (2019) also

hypothesized that flooding could be of higher magnitude during coupled negative AMO and PDO and positive AO and NAO phases, as in the case of the extraordinary 1936 winter flood in western Europe and eastern North America. The more positive phases of PDO since the 1970s are also consistent with more frequent El Niño events (Bonsal et al., 2001). Simulating the future of extreme La Niña and El Niño events under greenhouse gas warming by 2100, Cai et al. (2015) suggested that a greater number of extreme El Niño events would be compensated by La Niña events about twice as frequent as today. Such La Niña events may be associated with maximum spring discharge in our study. These simulations suggest that the frequency and magnitude of maximum spring discharge would continue to increase in our study area with future climatic changes.

The recent variability (especially in terms of frequency) of reconstructed spring discharge is therefore supported by climate variability. However, land use changes, or even beaver dams, may also have contributed to a lesser extent to the altering of regional runoff in the

river basins (Kundzewicz et al., 2019). Indeed, the increase in maximum discharge in the spring could be linked to an increase in runoff due to snowmelt through factors other than climate alone, such as through forest clear-cutting or urbanization. However, in the boreal forest of eastern Canada the settlement periods for large agricultural clearings and mine openings date from 1890 and 1910–1920 (Boileau, 1999), which does not correspond to the periods of change indicated by the reconstruction of spring discharge in the Harricana River (~1850 and 1950). In addition, Nolin et al. (2021), using flood rings as a flood proxy in four river basins distributed across northeastern Ontario and northwestern Québec, demonstrated the high spatial coherence among natural rivers and for the last 250 years (1770–2016). Their results suggest that the long-term variability observed in the spring flood signal is of climatic origin given the coherency observed over an area covering more than 70,000 km². The influence of non-climatic factors (land use changes, beaver dams, etc.) may be limited.

5. Conclusion

This study demonstrates the usefulness of developing continuous chronologies of earlywood vessels (and of visual flood-rings identification) for high-resolution reconstruction of annual spring discharge. The reconstructed Harricana River spring discharge is robust, with both low and high discharge years being equally well reconstructed. Ring-porous species growing in flood-prone environments and the plasticity of their anatomical features in response to stem submersion during annual spring flood demonstrated to be useful hydrological proxies. In a context where the period of flooding is sufficiently long and overlaps the period of earlywood vessels formation in submerged stems, year-to-year measurements of earlywood vessel areas should allow us to improve the understanding of long-term changes in regional spring discharge. Our high-resolution multi-century reconstruction of spring discharge provides evidence of increased high discharge since the end of the Little Ice Age. The likely cause is an increase in snow cover over much of central-east Canada rather than warmer air temperature. More work needs to be done to assess the stability of the association between REC1 and long-term circulation indices like ENSO, NAO and AMO. The strong spatial synchrony of the reconstructed spring discharge reconstruction with instrumental gauge data over a large territory in boreal Québec and Ontario for the later 20th and early 21st centuries suggests that the observed increase in the frequency and magnitude of flooding (high discharge), especially since the 1950s, is likely a consequence of climate change. Given the level of management and dam construction on rivers and the lack of hydrological data in northern Canada, paleohydrological studies using high-resolution tree-ring proxies are particularly relevant and need to be further developed.

Data availability

Relevant data for this study are available from Nolin, A. F., Tardif, J. C., Conciatori, F., Kames, S., Meko, D. M. & Bergeron, Y. (2021). *Fraxinus nigra* tree-ring dataset for dendrohydrology study in the Lake Duparquet, and reconstruction of the Harricana River spring discharge, Québec, Canada. *Mendeley Data*, v2, <https://doi.org/10.17632/d54gcxz9c5.2>. Data include earlywood vessels and tree-ring width chronologies derived from black ash (*Fraxinus nigra* Marsh.) trees growing in Lake Duparquet in eastern boreal Canada (Québec). *DUPARQUET_Chronologies.csv*, as in Fig. 2, the 12 anatomical and ring-width chronologies developed for Lake Duparquet to reconstruct Harricana River spring discharge; *DUPARQUET_lat_lon.kml*, the coordinate data for each station sampled on Lake Duparquet; *HARRICANA_rec&cal.csv*, as in Fig. 3A, the instrumental and reconstructed Harricana River spring discharge for the two models REC1 and REC2; *metadatas.txt*, a set of self-explanatory instructions and descriptions for data files. All other data are available upon request to the corresponding author at alexandre.florent.nolin@uqat.ca (institutional email), alexandreflorent.nolin@gmail.com (permanent email).

nolin@gmail.com (permanent email).

Declaration of Competing Interest

The authors declare no conflict of interest.

Acknowledgments

We thank the FERLD research station team and especially Danielle Charron and Raynald Julien for their continuous support over the two summers of field work. Great thanks go to the field assistants Cyrielle Ducrot, Chloé Lavelle, Isabelle Gareau and Stéphane Hébert as well as to The University of Winnipeg laboratory assistants Dominique Levin, Johanna R.M. Robson and Hollie Swart. We thank Yves Bégin, Étienne Boucher, Pierre Brigode, Mickaël Lemay, and Antoine Nicault for sharing their tree-ring hydrological reconstructions and for precious discussions on this project. This research is a contribution of the Canada Research Chairs (NSERC-CRC) held by YB and JT and was funded by a Natural Sciences and Engineering Research Council of Canada Collaborative research program including Ouranos, Hydro-Québec, Ontario Power Generation (OPG) and The University of Winnipeg. Earlier versions of the manuscript benefited from constructive comments by Jacinthe Clavet-Gaumont and David Huard (Ouranos) as well as from Kurt C. Kornelsen (OPG). We also acknowledge the contributions of the Editor-in-Chief (Pr. Jed O. Kaplan) and both reviewers (Pr. Juan A. Ballesteros-Cánovas and Pr. Matthew Therrell) who provided constructive comments and suggestions on earlier drafts of the manuscript.

Appendix A. Supplementary data

Supplementary data to this article can be found online at <https://doi.org/10.1016/j.gloplacha.2021.103444>.

References

- Agafonov, L.I., Meko, D.M., Panyushkina, I.P., 2016. Reconstruction of Ob River, Russia, discharge from ring widths of floodplain trees. *J. Hydrol.* 543, 198–207. <https://doi.org/10.1016/j.jhydrol.2016.09.031>.
- Astrade, L., Bégin, Y., 1997. Tree-ring response of *Populus tremula* L. and *Quercus robur* L. to recent spring floods of the Saône River, France. *ÉcoScience* 4 (2), 232–239.
- Aygün, O., Kinnard, C., Campeau, S., 2019. Impacts of climate change on the hydrology of northern midlatitude cold regions. *Prog. Phys. Geogr.* 1–38. <https://doi.org/10.1177/0309133319878123>.
- Baker, V.R., 2008. Paleoflood hydrology: Origin, progress, prospects. *Geomorphology* 101 (1–2), 1–13. <https://doi.org/10.1016/j.geomorph.2008.05.016>.
- Ballesteros-Cánovas, J.A., Stoffel, M., St. George, S., Hirschboeck, K., 2015. A review of flood records from tree rings. *Prog. Phys. Geogr.* 39 (6), 794–816. <https://doi.org/10.1177/0309133315608758>.
- Ballesteros-Cánovas, J.A., Stoffel, M., Benito, G., Rohrer, M., Barriopedro, D., García-Herrera, R., Brönnimann, S., 2019. On the extraordinary winter flood episode over the North Atlantic Basin in 1936. *Ann. N. Y. Acad. Sci.* 1436, 206–216. <https://doi.org/10.1111/nyas.13911>.
- Bégin, Y., 2000. Ice-push disturbances in high-boreal and subarctic lakeshore ecosystems since AD 1830, northern Québec, Canada. *The Holocene* 10 (2), 179–189.
- Bégin, Y., 2001. Tree-ring dating of extreme lake levels at the subarctic-boreal interface. *Quat. Res.* 55 (2), 133–139. <https://doi.org/10.1006/qres.2000.2203>.
- Bergeron, Y., Archambault, S., 1993. Decreasing frequency of forest fires in the southern boreal zone of Quebec and its relation to global warming since the end of the 'Little Ice Age'. *The Holocene* 3 (3), 255–259.
- Bergeron, Y., Gauthier, S., Kafka, V., Lefort, P., Lesieur, D., 2001. Natural fire frequency for the eastern Canadian boreal forest: consequences for sustainable forestry. *Can. J. For. Res.* 31 (3), 384–391. <https://doi.org/10.1139/x00-178>.
- Bergbuijs, W.R., Aalbers, E.E., Larsen, J.R., Trancoso, R., Woods, R.A., 2017. Recent changes in extreme floods across multiple continents. *Environ. Res. Lett.* 12 (11), 114,035. <https://doi.org/10.1088/1748-9326/aa8847>.
- Bilefsky, D., Austen, I., 2019, April 20. Eastern Canada Grapples with Extreme Flooding. The New-York Times. Retrieved from: <https://www.nytimes.com/2019/04/29/world/canada/canada-flooding.html> [2020, July 27].
- Biondi, F., Meko, D.M., 2019. Long-term hydroclimatic patterns in the Truckee-Carson basin of the eastern Sierra Nevada, USA. *Water Resour. Res.* 55 (7), 5559–5574. <https://doi.org/10.1029/2019WR024735>.
- Boileau, G., 1999. L'annexion du territoire de l'Abitibi au Québec. *Histoire Québec* 4 (2 bis), 30–33. <https://www.erudit.org/fr/revues/hq/1999-v4-n2-bis-hq1058506/11326ac.pdf>.

- Bonsal, B.R., Shabbar, A., Higuchi, K., 2001. Impacts of low frequency variability modes on Canadian winter temperature. *Int. J. Climatol.* 21, 95–108. <https://doi.org/10.1002/joc.590>.
- Bonsal, B.R., Prowse, T.D., Duguay, C.R., Lacroix, M.P., 2006. Impacts of large-scale teleconnections on freshwater-ice break/freeze-up dates over Canada. *J. Hydrol.* 330, 340–353. <https://doi.org/10.1016/j.jhydrol.2006.03.022>.
- Boucher, E., Ouarda, T.B.M.J., Bégin, Y., Nicault, A., 2011. Spring flood reconstruction from continuous and discrete tree ring series. *Water Resour. Res.* 47 (7), W07516. <https://doi.org/10.1029/2010WR010131>.
- Briffa, K.R., Jones, P.D., Pilcher, J.R., Hughes, M.K., 1988. Reconstructing summer temperatures in northern Fennoscandia back to AD 1700 using tree-ring data from Scots pine. *Arct. Alp. Res.* 20 (4), 385–394. <https://doi.org/10.2307/1551336>.
- Brigode, P., Brissette, F., Nicault, A., Perreault, L., Kuentz, A., Mathevet, T., Gailhard, J., 2016. Streamflow variability over the 1881–2011 period in northern Québec: comparison of hydrological reconstructions based on tree rings and geopotential height field reanalysis. *Clim. Past* 12 (9), 1785–1804. <https://doi.org/10.5194/cp-12-1785-2016>.
- Brown, R.D., 2010. Analysis of snow cover variability and change in Quebec, 1948–2005. *Hydroclim. Process.* 24, 1929–1954. <https://doi.org/10.1002/hyp.7565>.
- Bunn, A.G., 2008. A dendrochronology program library in R (dplR). *Dendrochronologia* 26 (2), 115–124. <https://doi.org/10.1016/j.dendro.2008.01.002>.
- Burn, D.H., Whitfield, P.H., 2015. Changes in floods and flood regimes in Canada. *Can. Water Res. J.* 41 (1–2), 139–150. <https://doi.org/10.1080/07011784.2015.1026844>.
- Burn, D.H., Whitfield, P.H., 2017. Changes in cold region flood regimes inferred from long-record reference gauging stations. *Water Resour. Res.* 53 (4), 2643–2658. <https://doi.org/10.1002/2016WR020108>.
- Burn, D.H., Whitfield, P.H., 2018. Changes in flood events inferred from centennial length streamflow data records. *Adv. Water Resour.* 121, 333–349. <https://doi.org/10.1016/j.advwatres.2018.08.017>.
- Burn, D.H., Whitfield, P.H., Sharif, M., 2016. Identification of changes in floods and flood regimes in Canada using a peak over threshold approach. *Hydroclim. Process.* 30 (18), 3303–3314. <https://doi.org/10.1002/hyp.10861>.
- Burton, I., 2015. Floods in Canada. *The Canadian Encyclopedia*. Retrieved from: www.thecanadianencyclopedia.ca/en/article/floods-and-flood-control [2020, July 27].
- Bush, E., Lemmen, D.S. (Eds.), 2019. *Canada's Changing Climate Report*. Government of Canada, Ottawa, ON, Canada (444 pp.).
- Buttle, J.M., Allen, D.M., Caisse, D., Davison, B., Hayashi, M., Peters, D.L., Pomeroy, J.W., Simonovic, S., St-Hilaire, A., Whitfield, P.H., 2016. Flood processes in Canada: regional and special aspects. *Can. Water Res. J.* 41 (1–2), 7–30. <https://doi.org/10.1080/07011784.2015.1131629>.
- Cai, W., Wang, G., Santosso, A., McPhaden, M.J., Wu, L., Jin, F.F., Timmermann, A., Collins, M., Vecchi, G., Lengaigne, M., England, M.H., Dommegget, D., Takahashi, K., Guilyardi, E., 2015. Increased frequency of extreme La Niña events under greenhouse warming. *Nat. Clim. Chang.* 5 (2), 132–137. <https://doi.org/10.1038/nclimate2492>.
- Canny, J., 1986. A computational approach to edge detection. *IEEE Trans. Pattern Anal. Mach. Intell.* PAMI-8 (6), 679–698. <https://doi.org/10.1109/TPAMI.1986.4767851>.
- Centre d'Expertise Hydraulique du Québec (CEHQ), 2019. Répertoire des barrages. Ministère de l'Environnement et de la Lutte contre les Changements climatiques. Gouvernement du Québec, Ottawa. Retrieved from: <https://www.cehq.gouv.qc.ca/barriages/default.asp> [February 12, 2020].
- Cherry, J.E., Knapp, C., Trainor, S., Ray, A.J., Tedesche, M., Walker, S., 2017. Planning for climate change impacts on hydropower in the Far North. *Hydroclim. Earth Syst. Sci.* 21 (1), 133–151. <https://doi.org/10.5194/hess-21-133-2017>.
- Clavet-Gaumont, J., Huard, D., Frigon, A., Koenig, K., Slota, P., Rousseau, A., Klein, I., Thiémonge, N., Houdré, F., Perdikaris, J., Turcotte, R., Lafleur, J., Larouche, B., 2017. Probable maximum flood in a changing climate: an overview for Canadian basins. *J. Hydrology Reg. Stud.* 13 (July), 11–25. <https://doi.org/10.1016/j.ejrh.2017.07.003>.
- Cook, E.R., Kairiukstis, L.A., 1990. *Methods of Dendrochronology - Applications in the Environmental Sciences* (Springer (ed.)). International Institute for Applied System Analysis (394 pp.) ISBN: 978-94-015-7879-0.
- Cook, E.R., Meko, D.M., Stahle, D.W., Cleaveland, M.K., 1999. Drought reconstructions for the continental United States. *J. Clim.* 12 (4), 1145–1163.
- Copini, P., Den Ouden, J., Robert, E.M.R., Tardif, J.C., Loesberg, W.A., Goudzwaard, L., Sasse-Klaassen, U., 2016. Flood-ring formation and root development in response to experimental flooding of young *Quercus robur* trees. *Front. Plant Sci.* 7 (June), 1–14. <https://doi.org/10.3389/fpls.2016.00775>.
- Daubois, V., Roy, M., Veillette, J.J., Ménard, M., 2015. The drainage of Lake Ojibway in glaciolacustrine sediments of northern Ontario and Quebec, Canada. *Boreas* 44 (2), 305–318. <https://doi.org/10.1111/bor.12101>.
- Davies, R., 2017, May 12. Canada – Over 4400 homes flooded in Quebec. Flood List. Retrieved from: <http://floodlist.com/americana-canada-flood-quebec-may-2017>.
- Denneler, B., Bergeron, Y., Bégin, Y., 1999. An attempt to explain the distribution of the tree species composing the riparian forests of Lake Duparquet, southern boreal region of Quebec, Canada. *Can. J. Bot.* 77 (12), 1744–1755. <https://doi.org/10.1139/jb-77-12-1744>.
- Denneler, B., Asselin, H., Bergeron, Y., Begin, Y., 2008. Decreased fire frequency and increased water levels affect riparian forest dynamics in southwestern boreal Quebec, Canada. *Can. J. For. Res.* 38 (5), 1083–1094. <https://doi.org/10.1139/X07-223>.
- Déry, S.J., Mlynowski, T.J., Hernández-Henríquez, M.A., Straneo, F., 2011. Interannual variability and interdecadal trends in Hudson Bay streamflow. *J. Mar. Syst.* 88 (3), 341–351. <https://doi.org/10.1016/j.jmarsys.2010.12.002>.
- Dickson, H.A., 2020. *Potential of Diffuse-Porous Tree Species in Dendrohydrology: Are Periodic Tangential Bands of Vessels the Equivalent of Flood Rings in Ring-Porous Tree Species?* Bachelor's Thesis, University of Winnipeg, Manitoba, Canada (80 pp.).
- Drobyshev, I., Bergeron, Y., Girardin, M.P., Gauthier, S., Ols, C., Ojal, J., 2017. Strong gradients in forest sensitivity to climate change revealed by dynamics of forest fire cycles in the post Little Ice Age era. *J. Geophys. Res. Biogeosci.* 122 (10), 2605–2616. <https://doi.org/10.1002/2017JG003826>.
- Efron, B., 1979. Bootstrap methods: another look at the jackknife. *Ann. Stat.* 7, 1–26.
- Environment and Climate Change Canada, 2020. Canada's Top 10 Weather Stories of 2019. Government of Canada, Toronto, Canada. Retrieved from: <https://www.canada.ca/en/environment-climate-change/services/top-ten-weather-stories/2019.html#toc2> [1 Sept 2020].
- Estilow, T.W., Young, A.H., Robinson, D.A., 2015. A long-term Northern Hemisphere snow cover extent data record for climate studies and monitoring. *Earth Syst. Sci. Data* 7 (1), 137. <https://doi.org/10.5194/esd-7-137-2015>.
- Fu, C., Yao, H., 2015. Trends of ice breakup date in south-central Ontario. *J. Geophys. Res.* 120 (18), 9220–9236. <https://doi.org/10.1002/2015JD023370>.
- García-González, I., Fonti, P., 2006. Selecting earlywood vessels to maximize their environmental signal. *Tree Physiol.* 26 (10), 1289–1296. <https://doi.org/10.1093/treephys/26.10.1289>.
- Gaur, A., Gaur, A., Simonovic, S.P., 2018. Future changes in flood hazards across Canada under a changing climate. *Water* 10, 1441. <https://doi.org/10.3390/w10101441>.
- Gaur, A., Gaur, A., Yamazaki, D., Simonovic, S.P., 2019. Flooding related consequences of climate change on canadian cities and flow regulation infrastructure. *Water* 11 (1), 63. <https://doi.org/10.3390/w11010063>.
- Gebre, S., Timalsina, N., Alfredsen, K., 2014. Some aspects of ice-hydropower interaction in a changing climate. *Energies* 7 (3), 1641–1655. <https://doi.org/10.3390/en7031641>.
- Gingras, D., Adamowski, K., Pilon, P.J., 1994. Regional flood equations for the provinces of Ontario and Quebec. *Water Resour. Bull.* 30 (1), 55–67. <https://doi.org/10.1111/j.1752-1688.1994.tb03273.x>.
- Girardin, M.P., Tardif, J.C., Flannigan, M.D., Bergeron, Y., 2006. Synoptic-scale atmospheric circulation and boreal Canada summer drought variability of the past three centuries. *J. Clim.* 19 (10), 1922–1947. <https://doi.org/10.1175/JCLI3716.1>.
- Griffin, D., Meko, D.M., Touchan, R., Leavitt, S.W., Woodhouse, C.A., 2011. Latewood chronology development for summer-moisture reconstruction in the US Southwest. *Tree-Ring Res.* 67 (2), 87–101. <https://doi.org/10.3959/2011-4.1>.
- Guay, C., Minville, M., Braun, M., 2015. A global portrait of hydrological changes at the 2050 horizon for the province of Québec. *Can. Water Res. J.* 40 (3), 285–302. <https://doi.org/10.1080/07011784.2015.1043583>.
- Gurrupu, S., St-Jacques, J.M., Sauchyn, D.J., Hodder, K.R., 2016. The influence of the Pacific Decadal Oscillation on annual floods in the rivers of western Canada. *JAWRA J. Am. Water Res. Assoc.* 52 (5), 1031–1045. <https://doi.org/10.1111/1752-1688.12433>.
- Harris, I., Osborn, T.J., Jones, P., Lister, D., 2020. Version 4 of the CRU TS monthly high-resolution gridded multivariate climate dataset. *Scientific Data* 7 (1), 1–18. <https://doi.org/10.1038/s41597-020-0453-3>.
- Hebbali, A., 2020. olrr: Tools for building Ordinary Least Square Regression Models. R package version 0.5.3. <https://cran-project.org/web/packages/olrr/index.html>.
- Hidalgo, H.G., Piechota, T.C., Dracup, J.A., 2000. Alternative principal components regression procedures for dendrohydrologic reconstructions. *Water Resour. Res.* 36 (11), 3241–3249. <https://doi.org/10.1029/2000WR000097>.
- Holmes, R.L., 1983. Computer-assisted quality control in tree-ring dating and measurement - COFECHA. *Tree-Ring Bull.* 43, 69–78.
- Hydro-Québec, 2019. Centrales électriques au 1er Janvier 2019. Retrieved from: <http://www.hydroquebec.com/production/centrale-hydroelectrique.html> [February 12, 2020].
- Insurance Bureau of Canada (IBC), 2020. Investing in Canada's future; the cost of climate adaptation at the local level. In: Final Report (February 2020). Canadian Municipalities, Federation of the (59 pp.).
- Javelle, P., Ouarda, T.B.M.J., Bobée, B., 2003. Spring flood analysis using the flood-duration-frequency approach: application to the provinces of Quebec and Ontario, Canada. *Hydroclim. Process.* 17, 3717–3736. <https://doi.org/10.1002/hyp.1349>.
- Jensen, O.P., Benson, B.J., Magnuson, J.J., Card, V.M., Futter, M.N., Soranno, P.A., Stewart, K.M., 2007. Spatial analysis of ice phenology trends across the Laurentian Great Lakes region during a recent warming period. *Limnol. Oceanogr.* 52 (5), 2013–2026. <https://doi.org/10.4319/lo.2007.52.5.2013>.
- Kames, S., Tardif, J.C., Bergeron, Y., 2016. Continuous earlywood vessels chronologies in floodplain ring-porous species can improve dendrohydrological reconstructions of spring high flows and flood levels. *J. Hydrol.* 534, 377–389. <https://doi.org/10.1016/j.jhydrol.2016.01.002>.
- Koshida, G., Cohen, S., Mortsch, L., 2015. Climate and water availability indicators in Canada: challenges and a way forward. Part I – indicators. *Can. Water Res. J.* 40 (2), 133–145. <https://doi.org/10.1080/07011784.2015.1006023>.
- Kundzewicz, Z.W., Szwed, M., Piiskwar, I., 2019. Climate variability and floods - a global review. *Water* 11 (7). <https://doi.org/10.3390/w11071399>.
- Larsson, L.A., 2003a. CDendro: Cybis Dendro Dating Program. Available at: <http://www.cybis.se>.
- Larsson, L.A., 2003b. CooRecorder: Image Co-Ordinate Recording Program. Available at: <http://www.cybis.se>.
- Legendre, P., Legendre, L., 2012. *Numerical Ecology (Development)* 3rd Edition. Elsevier (1006 pp.), ISBN: 978444538680.
- Lemay, M., Bégin, Y., 2008. Hydroclimatic analysis of an ice-scar tree-ring chronology of a high-boreal lake in Northern Québec, Canada. *Hydroclim. Process.* 39 (5–6), 451–464. <https://doi.org/10.1016/j.jhydrol.2008.0003>.

- Li, J., Xie, S.P., Cook, E.R., Morales, M.S., Christie, D.A., Johnson, N.C., Chen, F., D'Arrigo, R., Fowler, A.M., Gou, X., Fang, K., 2013. El Niño modulations over the past seven centuries. *Nat. Clim. Chang.* 3 (9), 822–826. <https://doi.org/10.1038/nclimate1936>.
- Lindenschmidt, K.E., Baulch, H.M., Cavalieri, E., 2018. River and lake ice processes - impacts of freshwater ice on aquatic ecosystems in a changing globe. *Water* 10 (11), 1586. <https://doi.org/10.3390/w10111586>.
- Ljungqvist, F.C., Krusic, P.J., Sundqvist, H.S., Zorita, E., Brattström, G., Frank, D., 2016. Northern Hemisphere hydroclimate variability over the past twelve centuries. *Nature* 532 (7597), 94–98. <https://doi.org/10.1038/nature17418>.
- López, J., Del Valle, J.I., Giraldo, J.A., 2014. Flood-promoted vessel formation in *Priaria copaifera* trees in the Darien Gap, Colombia. *Tree Physiol.* 34 (10), 1079–1089. <https://doi.org/10.1093/treephys/tpu077>.
- Martínez-Sifuentes, A.R., Villanueva-Díaz, J., Estrada-ávalos, J., 2020. Runoff reconstruction and climatic influence with tree rings, in the mayo river basin, Sonora, Mexico. *IForest* 13 (2), 98–106. <https://doi.org/10.3832/ifor3190-013>.
- Matthews, J.A., Briffa, K.R., 2005. The 'Little Ice Age': re-evaluation of an evolving concept. *Geografiska Annaler Ser A, Phys. Geo.* 87 (1), 17–36. <https://doi.org/10.1111/j.0435-3676.2005.00242.x>.
- McNeil, D.D., 2019. An Independent Review of the 2019 Flood Events in Ontario. Ontario's Special Advisor on Flooding Report to Government, a Report to the Hon. John Yakabuski, Minister of Natural Resources and Forestry (157 pp., Report no. 100546746-01). Retrieved from: <https://files.ontario.ca/mnrf-english-ontario-special-advisor-on-flooding-report-2019-11-25.pdf> [2020, Sept 10].
- Meko, D.M., Graybill, D.A., 1995. Tree-ring reconstruction of upper Gila River discharge. *J. Am. Water Resour. Assoc.* 31 (4), 605–616. <https://doi.org/10.1111/j.1752-1688.1995.tb03388.x>.
- Meko, D.M., Woodhouse, C.A., 2011. Application of streamflow reconstruction to water resources management. *Dendroclimatol. Develop. Paleoenvir. Res.* (11), 231–261. <https://doi.org/10.1007/978-1-4614-5725-0>.
- Meko, D.M., Therrell, M.D., Baisan, C.H., Hughes, M.K., 2001. Sacramento River flow reconstructed to AD 869 from tree rings. *JAWRA J. Am. Water Res. Assoc.* 37 (4), 1029–1039. <https://doi.org/10.1111/j.1752-1688.2001.tb05530.x>.
- Meko, D.M., Woodhouse, C.A., Morino, K., 2012. Dendrochronology and links to streamflow. *J. Hydrol.* 412, 200–209. <https://doi.org/10.1016/j.jhydrol.2010.11.041>.
- Meko, D.M., Panyushkina, I.P., Agafonov, L.A., Edwards, J.A., 2020. Impact of high flows of an Arctic river on ring widths of floodplain trees. *The Holocene* 30 (6), 789–798. <https://doi.org/10.1177/0959683620902217>.
- Meko, D.M., Therrell, M.D., 2020. A record of flooding on the White River, Arkansas derived from tree-ring anatomical variability and vessel width. *Phys. Geogr.* 41 (1), 83–98. <https://doi.org/10.1080/02723646.2019.1677411>.
- Mongrain, S., 2014. Dates de dégel du lac Duparquet. *Le Grand Héron: Le Journal de Duparquet*. 19 (1), 6.
- Mortsch, L., Cohen, S., Koshida, G., 2015. Climate and water availability indicators in Canada: challenges and a way forward. Part II – historic trends. *Can. Water Res. J.* 40 (2), 146–159. <https://doi.org/10.1080/07011784.2015.1006024>.
- Valley, D., Adamowski, J., Khalil, B., 2012. Using discrete wavelet transforms to analyze trends in streamflow and precipitation in Quebec and Ontario (1954–2008). *J. Hydrol.* 475, 204–228. <https://doi.org/10.1016/j.jhydrol.2012.09.049>.
- Nasri, B.R., Boucher, E., Perreault, L., Rémillard, B.N., Huard, D., Nicault, A., Members of the ARCHIVES-PERSISTENCE projects, 2020. Modeling hydrological inflow persistence using paleoclimate reconstructions on the Québec-Labrador (Canada) Peninsula. *Water Resour. Res.* 56, e2019WR025122. <https://doi.org/10.1029/2019WR025122>.
- Nicault, A., Boucher, E., Bégin, C., Guiot, J., Marion, J., Perreault, L., Roy, R., Savard, M. M., Bégin, Y., 2014. Hydrological reconstruction from tree-ring multi-proxies over the last two centuries at the Caniapiscau Reservoir, northern Québec, Canada. *J. Hydrol.* 513, 435–445. <https://doi.org/10.1016/j.jhydrol.2014.03.054>.
- Nolin, A.F., Tardif, J.C., Conciatori, F., Bergeron, Y., 2021. Spatial coherency of the spring flood signal among major river basins of eastern boreal Canada inferred from flood rings. *J. Hydrol.*
- Ontario Ministry of Natural Resources and Forestry (OMNRF), 2019. Ontario Dam Inventory. Provincial Mapping Unit, Government of Ontario, Toronto. Retrieved from: <https://geohub.lio.gov.on.ca/datasets/mnrf:ontario-dam-inventory> [February 12, 2020].
- Ontario Power Generation (OPG), 2019. River System Data. Retrieved from: <https://www.opp.com/powering-ontario/our-generation/hydro/river-system-data/> [February 12, 2020].
- Payette, S., 1980. Major ice floods on the Leaf River (Nouveau-Québec): a dendrochronological analysis. *Nat. Can.* 107 (4), 215–225.
- Pellerin, J.E., 2019. Updating the Canadian Reference Hydrometric Basin Network to Detect Climate-Related Trends in Streamflow. Master's thesis, University of Waterloo. https://uwspace.uwaterloo.ca/bitstream/handle/10012/14574/Pellerin_Jennifer.pdf?sequence=5&isAllowed=y.
- Phipps, R.L., 1985. Collecting, preparing, crossdating, and measuring tree increment cores. In: U.S. Geological Survey. <https://doi.org/10.3133/wri854148>. Water Resources Investigations Report 85-4148, 48 pp.
- R Core Team, 2020. R: A Language and Environment for Statistical Computing. R Foundation for Statistical Computing, Vienna, Austria. <https://R-project.org/>.
- Régent Instruments Inc, 2018. WinCell Pro Version 2018c User Manual. Québec, Québec.
- Rodionov, S., Assel, R.A., 2003. Winter severity in the Great Lakes region: a tale of two oscillations. *Clim. Res.* 24 (1), 19–31. <https://doi.org/10.3354/cr024019>.
- Roesch, A., Schmidbauer, H., 2018. WaveletComp: Computational Wavelet Analysis. R package version 1.1. <https://cran.r-project.org/web/packages/WaveletComp/index.html>.
- Rueden, C.T., Schindelin, J., Hiner, M.C., DeZonia, B.E., Walter, A.E., Arena, E.T., Elceir, K.W., 2017. ImageJ2: ImageJ for the next generation of scientific image data. *BMC Bioinform.* 18 (529), 1–26. <https://doi.org/10.1186/s12859-017-1934-z>.
- Saint-Laurent, D., 2004. Palaeoflood hydrology: an emerging science. *Prog. Phys. Geogr.* 28 (4), 531–543. <https://doi.org/10.1191/0309133304pp423oa>.
- Scholz, A., Klepsch, M., Karimi, Z., Jansen, S., 2013. How to quantify conduits in wood? *Front. Plant Sci.* 4 (MARCH), 1–11. <https://doi.org/10.3389/fpls.2013.00056>.
- Snee, R.D., 1977. Validation of regression models: methods and examples. *Technometrics* 19 (4), 415–428. <https://doi.org/10.1080/00401706.1977.10489581>.
- St. George, S., Nielsen, E., 2000. Signatures of high-magnitude 19th-Century floods in *Quercus macrocarpa* tree rings along the Red River, Manitoba, Canada. *Geology* 28 (10), 899–902. [https://doi.org/10.1130/0091-7613\(2000\)28<899:SOHTFI>2.0.CO;2](https://doi.org/10.1130/0091-7613(2000)28<899:SOHTFI>2.0.CO;2).
- St. George, S., Nielsen, E., 2003. Palaeoflood records for the Red River, Manitoba, Canada, derived from anatomical tree-ring signatures. *The Holocene* 13 (4), 547–555. <https://doi.org/10.1191/0959683603hl645rp>.
- St. George, S., Nielsen, E., Conciatori, F., Tardif, J., 2002. Trends in *Quercus macrocarpa* vessel areas and their implications for tree-ring paleoflood studies. *Tree-Ring Res.* 58, 3–10.
- Tardif, J.C., 1996. Earlywood, latewood and total ring width of a ring-porous species (*Fraxinus nigra* Marsh.) in relation to climate and hydrologic factors. In: *Tree rings, environment and humanities*. In: Dean, J.S., Meko, D.M., Swetnam, T.W. (Eds.), *Radiocarbon*. University of Arizona, Tucson, pp. 315–324.
- Tardif, J.C., Bergeron, Y., 1992. Analyse écologique des peuplements de frêne noir (*Fraxinus nigra*) des rives du lac Duparquet, nord-ouest du Québec. *Can. J. Bot.* 70 (11), 2294–2302. <https://doi.org/10.1139/b92-285>.
- Tardif, J.C., Bergeron, Y., 1993. Radial growth of *Fraxinus nigra* in a Canadian boreal floodplain in response to climatic and hydrological fluctuations. *J. Veg. Sci.* 4 (6), 751–758. <https://doi.org/10.2307/2325611>.
- Tardif, J.C., Bergeron, Y., 1997a. Comparative dendroclimatological analysis of two black ash and two white cedar populations from contrasting sites in the Lake Duparquet region, northwestern Quebec. *Can. J. For. Res.* 27, 108–116. <https://doi.org/10.1139/x96-150>.
- Tardif, J.C., Bergeron, Y., 1997b. Ice-flood history reconstructed with tree-rings from the southern boreal forest limit, western Quebec. *The Holocene* 7 (3), 291–300. <https://doi.org/10.1177/095968369700700305>.
- Tardif, J.C., Bergeron, Y., 1999. Population dynamics of *Fraxinus nigra* in response to flood-level variations, in northwestern Québec. *Ecol. Monogr.* 69 (1), 107–125. [https://doi.org/10.1890/0012-9615\(1999\)069\[0107:PDONF\]2.0.CO;2](https://doi.org/10.1890/0012-9615(1999)069[0107:PDONF]2.0.CO;2).
- Tardif, J.C., Conciatori, F., 2006. Influence of climate on tree rings and vessel features in red oak and white oak growing near their northern distribution limit, southwestern Quebec, Canada. *Can. J. For. Res.* 36 (9), 2317–2330. <https://doi.org/10.1139/x06-133>.
- Tardif, J.C., Dutilleul, P., Bergeron, Y., 1998. Variations in periodicities of the ring width of black ash (*Fraxinus nigra* Marsh.) in relation to flooding and ecological site factors at Lake Duparquet in northwestern Quebec. *Biol. Rhythms* 29 (1), 1–29. <https://doi.org/10.1076/brrh.29.1.1.3040>.
- Tardif, J.C., Kames, S., Bergeron, Y., 2010. Spring water levels reconstructed from ice-scarsred trees and cross-sectional area of the earlywood vessels in tree-rings from eastern boreal Canada. In: Stoffel, M., Bollscheiwer, M., Butler, D.R., Luckman, B.H. (Eds.), *Tree-Rings and Natural Hazards: A State-of-Art, Advances in Global Change Research*, vol. 41. Springer, pp. 257–261.
- Tardif, J.C., Kames, S., Conciatori, F., Bergeron, Y., 2016. Developing continuous earlywood vessels chronologies in ring-porous species can improve dendrohydrological reconstructions of spring high flows and flood levels. In: *Third American Dendrochronology Conference - Dendrohydrology Session*, pp. 50–51.
- Therrell, M.D., Bialecki, M.B., 2015. A multi-century tree-ring record of spring flooding on the Mississippi River. *J. Hydrol.* 529 (P2), 490–498. <https://doi.org/10.1016/j.jhydrol.2014.11.005>.
- Torrance, C., Compo, G.P., 1998. A practical guide to wavelet analysis. *Bull. Am. Meteorol. Soc.* 79 (1), 61–78. [https://doi.org/10.1175/1520-0477\(1998\)079<0061:APGTTWA>2.0.CO;2](https://doi.org/10.1175/1520-0477(1998)079<0061:APGTTWA>2.0.CO;2).
- Trouet, V., Van Oldenborgh, G.J., 2013. KNMI Climate Explorer: a web-based research tool for high-resolution paleoclimatology. *Tree-Ring Res.* 69 (1), 3–13. <https://doi.org/10.3959/1536-1098-69.1.3>.
- Turcoote, B., Burrell, B.C., Beltaos, S., 2019. The impact of climate change on breakup ice jams in Canada: state of knowledge and research approaches. CGU HS Committee on river ice processes and the environment. In: *20th Workshop on the Hydraulics of ice Covered Rivers*, Ottawa, Ontario, Canada, May 14–16, 2019.
- Tyree, M.T., Zimmermann, M.H., 2002. *Xylem Structure and the Ascent of Sap*, 2nd edn. Springer, Verlag, Berlin, Germany.
- Vincent, L.A., Zhang, X., Mekis, É., Wan, H., Bush, E.J., 2018. Changes in Canada's climate: trends in indices based on daily temperature and precipitation data. *Atmosphere-Ocean* 56 (5), 332–349. <https://doi.org/10.1080/0705900.2018.1514579>.
- Wang, X., Huang, G., Liu, J., Li, Z., Zhao, S., 2015. Ensemble projections of regional climatic changes over Ontario, Canada. *J. Clim.* 28 (18), 7327–7346. <https://doi.org/10.1175/JCLI-D-15-0185.1>.
- Wertz, E.L., St. George, S., Zeleznik, J.D., 2013. Vessel anomalies in *Quercus macrocarpa* tree rings associated with recent floods along the Red River of the North, United States. *Water Resour. Res.* 49 (1), 630–634. <https://doi.org/10.1029/2012WR012900>.
- Wigley, T.M.L., St. George, S., Briffa, K.R., Jones, P.D., 1984. On the average value of correlated time series with applications in dendroclimatology and hydrometeorology. *J. Clim. Appl. Meteorol.* 23 (2), 201–213. [https://doi.org/10.1175/1520-0450\(1984\)023<0201:OTAVOC>2.0.CO;2](https://doi.org/10.1175/1520-0450(1984)023<0201:OTAVOC>2.0.CO;2).

- Wilhelm, B., Ballesteros-Cánovas, J.A., Macdonald, N., Toonen, W.H.J., Baker, V., Barriendos, M., Benito, G., Brauer, A., Corella, J.P., Denniston, R., Glaser, R., Ionita, M., Kahle, M., Liu, T., Luetscher, M., Macklin, M., Mudelsee, M., Muñoz, S., Schulte, L., St. George, S., Stoffel, M., Wetter, O., 2019. Interpreting historical, botanical, and geological evidence to aid preparations for future floods. Wiley Interdiscip. Rev. Water 6 (1), e1318. <https://doi.org/10.1002/wat2.1318>.
- Winsemius, H.C., Aerts, J.C., van Beek, L.P., Bierkens, M.F., Bouwman, A., Jongman, B., Kwadijk, J.C.J., Ligtnvoet, W., Lucas, P.L., van Vuuren, D.P., Ward, P.J., 2016. Global drivers of future river flood risk. Nat. Clim. Chang. 6 (4), 381–385. <https://doi.org/10.1038/nclimate2893>.
- Woodhouse, C.A., Grey, S.T., Meko, D.M., 2006. Updated streamflow reconstructions for the Upper Colorado River Basin. Water Resour. Res. 42 (5), 1–16. <https://doi.org/10.1029/2005WR004455>.
- Zang, C., Biondi, F., 2015. treeclim: an R package for the numerical calibration of proxy-climate relationships. Ecography 38 (4), 431–436. <https://doi.org/10.1111/ecog.01335>.
- Zhang, W., Mei, X., Geng, X., Turner, A.G., Jin, F.F., 2019. A nonstationary ENSO–NAO relationship due to AMO modulation. J. Clim. 32 (1), 33–43. <https://doi.org/10.1175/JCLI-D-18-0365.1>.
- Zhao, H., Higuchi, K., Waller, J., Auld, H., Mote, T., 2013. The impacts of the PNA and NAO on annual maximum snowpack over southern Canada during 1979–2009. Int. J. Climatol. 33 (2), 388–395. <https://doi.org/10.1002/joc.3431>.